Article

Immunity

Structural Damage in the *C. elegans* Epidermis Causes Release of STA-2 and Induction of an Innate Immune Response

Highlights

- Epidermal structural damage induces AMP transcription in the *C. elegans* epidermis
- The epidermal immune system senses structural damage through hemidesmosomes
- Hemidesmosomes regulate AMP transcription through association with STAT proteins
- Hemidesmosome disassembly in HEKa cells induces transcription of β-defensin AMPs

Authors

Yun Zhang, Wenna Li, ..., Sidong Xiong, Huimin Zhang

Correspondence

sdxiong@suda.edu.cn (S.X.), zhanghuimin@suda.edu.cn (H.Z.)

In Brief

Little is known about the connection between epidermal structures and immune regulatory function. Zhang and colleagues report on a STAT-based immune defense machinery embedded within the epidermal architecture and show that it senses the disruption of stable adhesion complexes and activates transcription of antimicrobial peptides upon internal or external insults.

Zhang et al., 2015, Immunity *42*, 309–320
February 17, 2015
http://dx.doi.org/10.1016/j.immuni.2015.01.014

CellPress

Immunity
Article

Structural Damage in the *C. elegans* Epidermis Causes Release of STA-2 and Induction of an Innate Immune Response

Yun Zhang,[1] Wenna Li,[1] Linfeng Li,[1] Yuanbao Li,[1] Rong Fu,[1] Yi Zhu,[1] Jie Li,[1] Yanfeng Zhou,[1] Sidong Xiong,[1,*] and Huimin Zhang[1,*]
[1]Jiangsu Key Laboratory of Infection and Immunity, Institutes of Biology and Medical Sciences, Soochow University, Suzhou, Jiangsu 215123, China
*Correspondence: sdxiong@suda.edu.cn (S.X.), zhanghuimin@suda.edu.cn (H.Z.)
http://dx.doi.org/10.1016/j.immuni.2015.01.014

SUMMARY

The epidermis constantly encounters invasions that disrupt its architecture, yet whether the epidermal immune system utilizes damaged structures as danger signals to activate self-defense is unclear. Here, we used a *C. elegans* epidermis model in which skin-penetrating infection or injury activates immune defense and antimicrobial peptide (AMP) production. By systemically disrupting each architectural component, we found that only disturbance of the apical hemidesmosomes triggered an immune response and robust AMP expression. The epidermis recognized structural damage through hemidesmosomes associated with a STAT-like protein, whose disruption led to detachment of STA-2 molecules from hemidesmosomes and transcription of AMPs. This machinery enabled the epidermis to bypass certain signaling amplification and directly trigger AMP production when subjected to extensive architectural damage. Together, our findings uncover an evolutionarily conserved mechanism for the epithelial barriers to detect danger and activate immune defense.

INTRODUCTION

Being a physical barrier and frontline defense, the epidermis is in constant confrontation against pathological or mechanical insults. Many of such insults eventually disrupt the architecture of the epidermal cells. Increasing evidence provided by models of vertebrate or invertebrate skin has linked structural damage with epidermal innate defense and skin inflammation. Specifically, sterile mechanical wounding upon the skin of human, *Drosophila melanogaster*, or *Caenorhabditis elegans* can elicit an innate immune response in the epidermis, which leads to elevated production of antimicrobial peptides (AMPs) by epidermal cells (De Gregorio et al., 2002; Patterson et al., 2013; Pujol et al., 2008a; Sørensen et al., 2006). Such innate defense is usually independent of the wound-healing process, possibly to help prepare against inevitable pathogen invasion following breach of the epidermal barrier (Davis and Engström, 2012; Xu and Chisholm, 2011). In addition, genetic mutations targeting internal structural components of the epidermal cells often result in inflammation in the mammalian skin (Niculescu et al., 2011; Perez-Moreno et al., 2006; Perez-Moreno et al., 2008; Sandilands et al., 2009). However, it is difficult to determine whether such inflammatory response is triggered directly by structural damage of the epidermal cells or indirectly by infiltration of pathogens, allergens, or specialized immune cells. It is equally unclear whether the epidermal cells across species can recognize such disturbance of architectural integrity as a type of danger signal for immediate activation of immune response. In sum, the links between architectural damage and epidermal innate immune defense remain poorly defined.

The *C. elegans* epidermis provides an excellent model for understanding basic innate defense strategies of the epithelial tissues. The adult *C. elegans* epidermis is a thin, single-celled epithelial barrier enclosing the internal organs and is formed mostly by one multi-nuclear syncytium named the hyp7 cell (Chisholm and Xu, 2012). The shape and thickness of the *C. elegans* epidermal layer is mainly supported by the rigid cuticle exoskeleton at the apical side and the four wide muscle quadrants at the basal side. The transepidermal *C. elegans* hemidesmosomes (hereby referred to as CeHDs) attach the epidermal cells apically to the cuticle and basally to the basement extracellular matrix (ECM). The apical and basal CeHD units connect the cuticle, epidermis, and muscle layers through intermediate filaments (IFs) (Zhang and Labouesse, 2010). The microtubule cytoskeletons form long, thick bundles that span the entire epidermis and provide mechanical support intracellularly. A network of actin-linked apical cytoskeleton made of spectrins also helps maintain epidermal shape (Pasti and Labouesse, 2014).

The *C. elegans* epidermal cells possess cell-autonomous defense machineries against invading pathogens or physical injury. *Drechmeria coniospora*, a representative skin-penetrating fungus, produces conidia that adhere and pierce the cuticle to spread hyphae into the worm body. Such invasion activates G protein signaling through G-protein-coupled receptor DCAR-1 and transduces signals via a conserved p38-MAPK signaling cassette (Ziegler et al., 2009; Zugasti et al., 2014). As a result of the innate immune response, a group of AMPs known as neuropeptide-like proteins (NLPs) are upregulated in the epidermis. Both the GATA transcription factor ELT-3 and the STAT family protein STA-2 are partially required for the upregulation of NLP family AMPs (Dierking et al., 2011; Pujol et al., 2008b). The

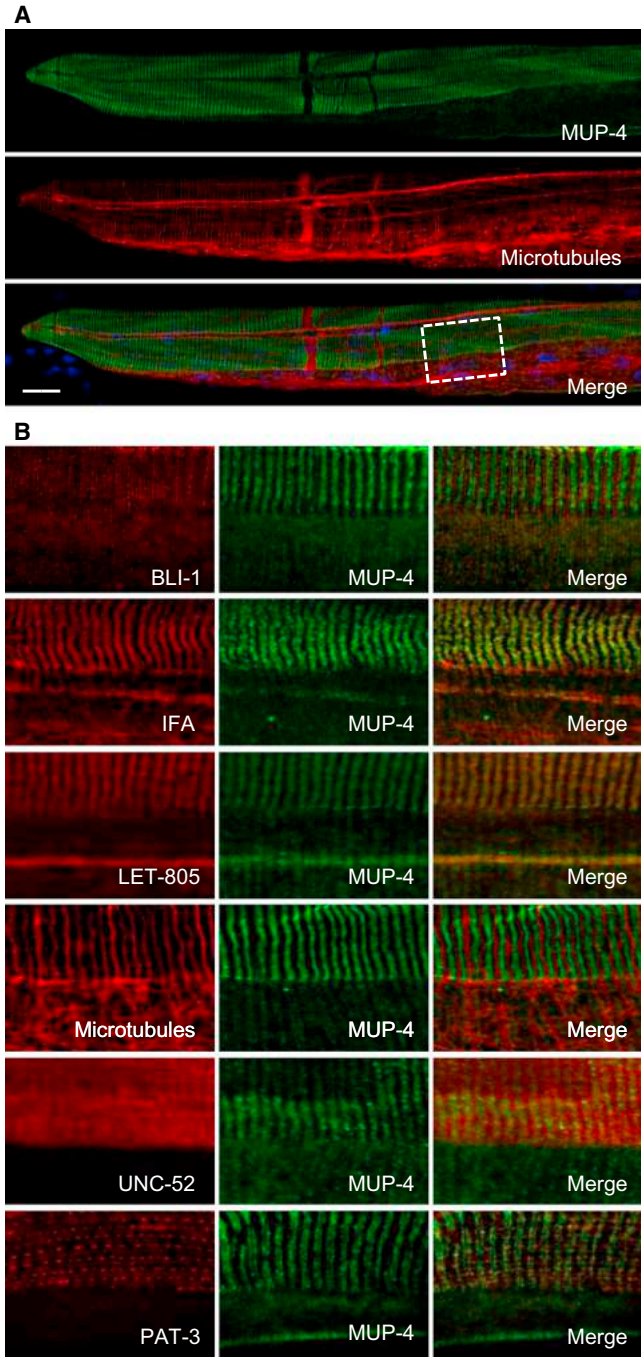

Figure 1. The Spatial Distribution of Supporting Structures in the *C. elegans* Epidermis Is Highly Organized

(A) A composite confocal image shows the anterior half of a wild-type L4 hermaphrodite stained with antibodies against microtubules (red) and apical CeHD receptor MUP-4 (green). DAPI (blue) was used to counterstain nuclei. The scale bar represents 25 μm.

(B) Double labeling of reference landmark MUP-4 (green) and other epidermal-related structural components (red) in regions corresponding to the boxed area in (A). The structures are as follows: struts that anchor the epidermal cells to the outer cuticle (BLI-1), apical CeHDs (MUP-4), intermediate filaments that connect apical and basal CeHDs (IFA), basal CeHDs (LET-805), microtubules (α-tubulin), basal ECM (UNC-52), and muscle dense bodies (PAT-3).

See also Figure S1.

anti-fungal immune response also upregulates Caenacin family AMPs through independent transforming growth factor β (TGF-β) signaling derived from neurons (Zugasti and Ewbank, 2009). Sterile wounding of the epidermis by a microinjection needle or femtosecond laser induces AMP transcription through pathways overlapping those involved in anti-fungal defense. DCAR-1, G protein signaling, p38-MAPK signaling, and STA-2 are all required for proper induction of the AMPs after mechanical wounding (Dierking et al., 2011; Pujol et al., 2008a; Ziegler et al., 2009; Zugasti et al., 2014). The transcription of epidermal AMPs can also be elevated by hyperosmotic stress mediated by the WNK-Ste20 pathway, which senses cell volume change (Chisholm and Xu, 2012; Lee et al., 2010). The major pattern-recognition receptors in *C. elegans* epidermal cells have not yet been identified. It is also unclear how the epidermal innate immune system recognizes signals produced by physical injury. Although physical wounding induces rapid elevation of Ca^{2+} flux and a wound-closure response, the Ca^{2+} signal and the wound-healing process appear to not be required for the activation of immune defense (Xu and Chisholm, 2011). Recent progress has shown that the G-protein-coupled receptor DCAR-1, activated by an endogenous tyrosine metabolite hydroxyphenyllactic acid (HPLA), acts upstream of p38-MAPK to induce epidermal AMP expression. Yet, the link between physical injury and production of HPLA still remains unknown (Zugasti et al., 2014).

Here, we utilized *C. elegans* epidermis as the model skin and systemically investigated the involvement of epidermal supporting structures in damage-induced innate immune response under pathogen-free conditions. We identified a group of structural components clustered around apical CeHD receptor MUP-4 and found that they could initiate innate immune response once damaged. Further investigation revealed that the epidermis sensed its internal structural disturbance through a STAT protein tethered to the stable attachment structures at the apical membrane. The association between STA-2 and hemidesmosomes enabled the epidermis to quickly respond to extensive physical damage without the need to go through multiple signaling cascades. Our study reveals a simple and energy-efficient innate defense machinery embedded inside the mechanical architecture of the epidermal cells and an evolutionally conserved strategy for the epidermis to sense danger through its internal structures.

RESULTS

C. elegans Epidermal Structures Display Highly Organized Spatial Distribution Patterns

To identify the structural components involved in damage-induced epidermal immune response, we first mapped out the relative positions of major supporting structures composing the epidermal architecture of *C. elegans* (Figure 1). Specifically, cuticle struts, apical CeHDs, basal CeHDs, intermediate filaments, microtubule bundles, basement ECM, and muscle dense bodies were marked by antibodies against BLI-1, MUP-4, LET-805, IFA-2/3, α-tubulin, UNC-52, and PAT-3, respectively (Gettner et al., 1995; Hong et al., 2001; Hresko et al., 1999; Lints and Hall, 2009; McMahon et al., 2003; Mullen et al., 1999). The apical CeHD transmembrane protein MUP-4 was used as a reference landmark (Hong et al., 2001). Immunostaining of MUP-4 showed

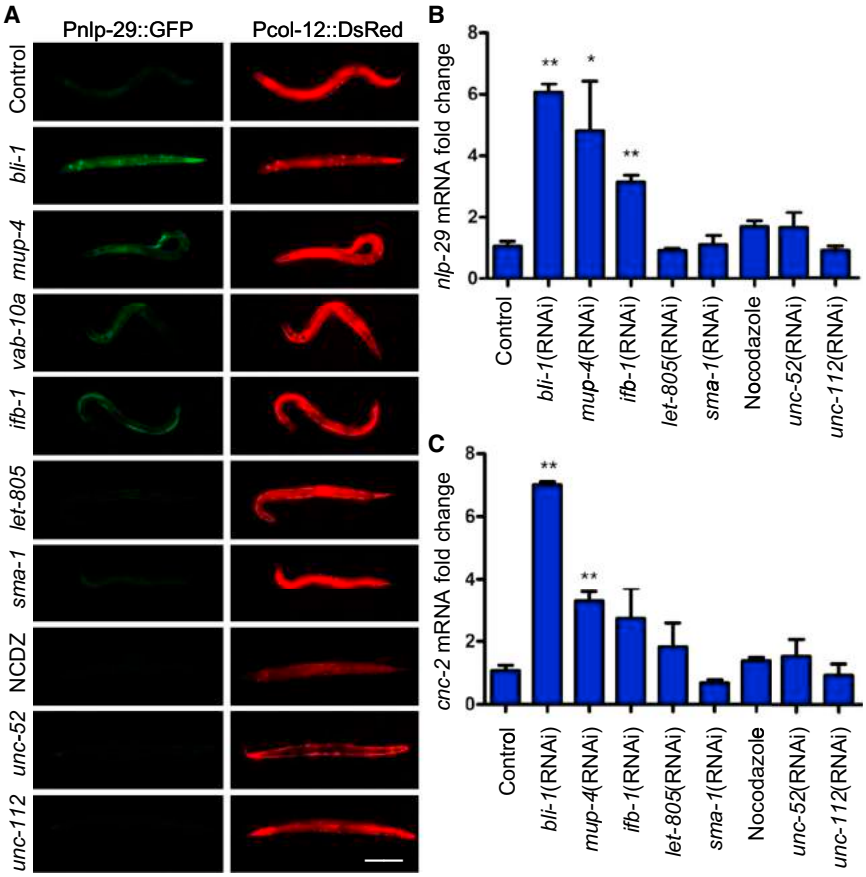

Figure 2. Disruption of Epidermal Architecture Induces AMP Expression in a Spatially Restricted Manner

(A) Expression of Pnlp-29::GFP after damage of struts (*bli-1*), apical CeHDs (*mup-4*), plakin cytolinker (*vab-10a*), intermediate filaments (*ifb-1*), basal CeHDs (*let-805*), apical cytoskeleton (*sma-1*), microtubules (NCDZ), basal ECM (*unc-52*), and muscle dense bodies and M-lines (*unc-112*). Pcol-12::DsRed served as an internal control. NCDZ stands for nocodazole. The scale bar represents 200 μm.

(B and C) Quantitative RT-PCR results show *nlp-29* or *cnc-2* expression in worms after deletion of various epidermal supporting structures. Error bars represent the mean ± SEM (three biological replicates, n ≥ 100/condition). Asterisks denote a significant increase in AMP expression in comparison to the control (*$p < 0.05$, **$p < 0.01$).

See also Figure S2.

that the apical CeHD foci were organized into paralleled stripes located in between cuticle furrows. The BLI-1-labeled struts, which connect the epidermis with the outer cuticle layer, also formed paralleled stripes and were positioned in between and overlapping CeHD stripes. The basal CeHD transmembrane protein LET-805 mostly co-localized with MUP-4 but was only restricted to the area overlaying muscles, whereas anti-MUP-4 also displayed faint staining outside of the muscle-attached area. Intermediate filaments stained by anti-IFA co-localized with CeHDs. In contrast, microtubule bundles were only positioned between the gaps of CeHD stripes. Actin filaments in the epidermis do not organize into bundles except before each molting period (Costa et al., 1997). The major basement ECM component UNC-52 and the muscle attachment receptor PAT-3 exhibited no obvious spatial correlations with the CeHDs. In general, most epidermal supporting structures were organized into parallel stripe patterns and displayed minimum entanglement (Figure 1B and Figures S1A–S1C). This highly ordered 3D architecture allowed us to perform targeted destruction of one structure at a time without causing extensive collateral damage.

Epidermal Architectural Damage Induces AMP Transcription in a Spatially Restricted Manner

We next disrupted individual epidermal supporting structures by RNAi or drug treatment (Figure 2 and Figure S2). Specifically, struts of the cuticle exoskeleton, apical CeHDs, plakin cytolinker, intermediate filaments, basal CeHDs, actin-linked apical cytoskeleton, basal ECM, and muscle quadrants were each destroyed by inactivation of *bli-1*, *mup-4*, *vab-10a*, *ifb-1*, *let-805*, *sma-1*, *unc-52*, and *unc-112*, respectively (Bosher et al., 2003; Hong et al., 2001; Hresko et al., 1999; Lints and Hall, 2009; McKeown et al., 1998; Mullen et al., 1999; Rogalski et al., 2000; Woo et al., 2004). Polymerization of microtubule bundles was inhibited by nocodazole treatment. Their effects on innate immune response were then analyzed by examination of the expression of *nlp-29* and *cnc-2*, genes representing two major AMP families produced in the epidermis (Chisholm and Xu, 2012). Both transcriptional GFP reporter and qPCR analyses were used for evaluating AMP expression. Consistent with reports that inactivation of genes encoding actin or tubulin cytoskeletons does not affect *nlp-29* expression, *sma-1* RNAi or nocodazole treatment did not induce AMP production (Figure 2A) (Melo and Ruvkun, 2012). Likewise, damage of most other aforementioned epidermal supporting structures, except for the components within or associated with apical CeHDs, did not upregulate *nlp-29* or *cnc-2* (Figure 2 and Figure S2). Specifically, inactivation of apical CeHD receptor *mup-4* or its extracellular partner *bli-1* triggered robust AMP production (Figure 2 and Figures S2B and S2C). Knockdown of *ifb-1*, encoding the intermediate filament protein that associates with CeHD attachments, resulted in moderate *nlp-29* upregulation (Figures 2A and 2B). Loss of VAB-10A, the cytolinker that helps connect CeHDs to the IFs, also mildly induced *nlp-29* transcription (Figures 2A and 3A and Figure S2D) (Bosher et al., 2003). In summary, the collapse of the epidermal architecture itself was not sufficient to trigger an innate defense. Only damage of the apical CeHDs and their neighboring structures could induce an epidermal immune response and AMP production.

The Apical CeHD Transmembrane Protein MUP-4 Is a Key Component of Immune Activation

Each transepidermal CeHD unit is a highly complex adhesion structure formed by multiple components (Figure S1D). To

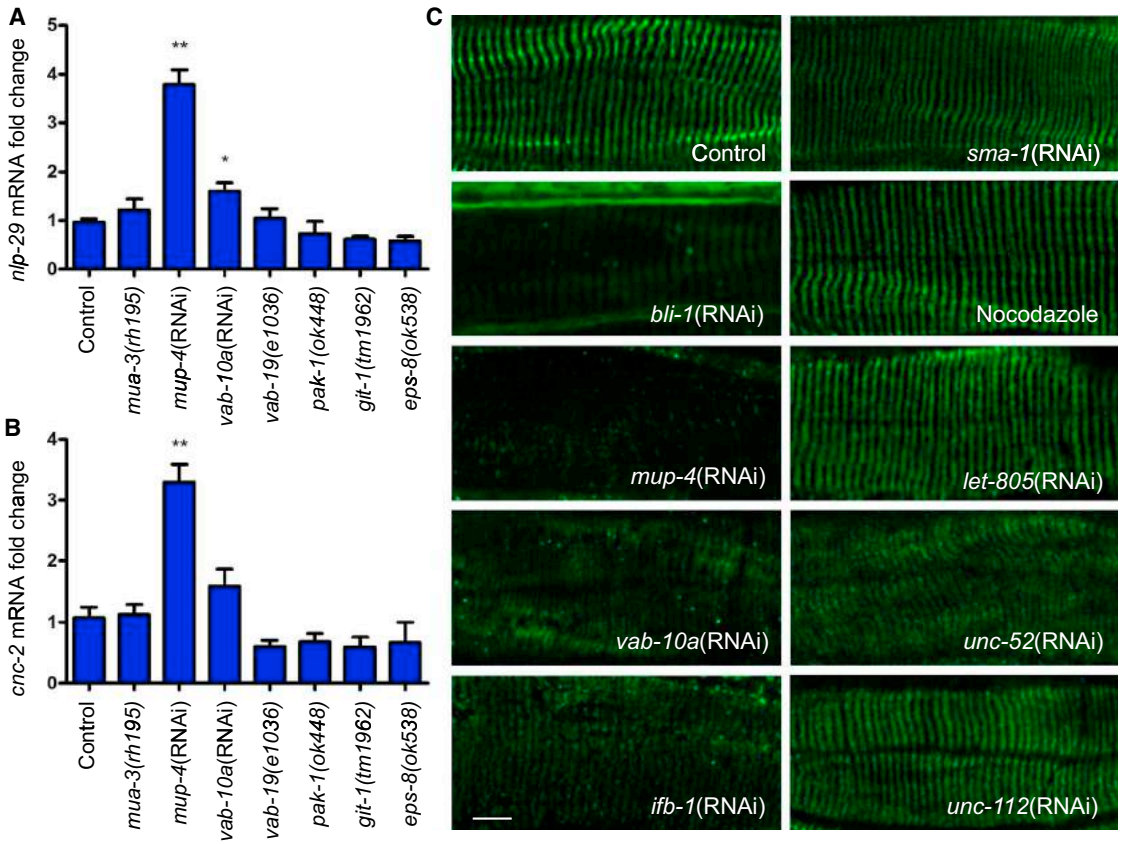

Figure 3. Disruption of the Apical CeHD Receptor MUP-4 Induces AMP Production

(A and B) Quantitative RT-PCR results show *nlp-29* or *cnc-2* expression in worms lacking different CeHD components. Error bars represent the mean ± SEM (three biological replicates, n ≥ 100/condition). Asterisks denote a significant increase in AMP expression in comparison to the control (*p < 0.05, **p < 0.01). (C) Representative confocal images of MUP-4 immunostaining in L4 hermaphrodites with damaged struts (*bli-1*), apical CeHDs (*mup-4*), cytolinker (*vab-10*), epidermal cytoskeletons (*ifb-1*, *sma-1*, and Nocodazole), basal CeHDs (*let-805*), basal ECM (*unc-52*), or muscle structures (*unc-112*). The scale bar represents 10 μm.

See also Figure S3.

investigate which CeHD components contribute to the induction of AMP expression, we utilized RNAi or loss-of-function mutations to inactivate most CeHD-related genes (Zhang and Labouesse, 2010; Zhang et al., 2011). Compared to loss of *mup-4*, loss of most other CeHD components did not dramatically increase *nlp-29* or *cnc-2* expression, even though some of those mutations, such as *mua-3(rh195)* or *vab-19(e1036)*, affected the structural integrity of the epidermis (Figures 3A and 3B) (Bercher et al., 2001; Ding et al., 2003). Therefore, it appears that the apical CeHD receptor MUP-4 is the main player responsible for AMP production in the epidermis.

We then explored the possibility that loss of *bli-1* and *ifb-1* induces *nlp-29* expression by indirectly affecting MUP-4 organization at the CeHDs. We analyzed changes of MUP-4 localization in the epidermis after disruption of different epidermal structures by immunostaining. In general, the severity of MUP-4 disruption correlated with the degree of AMP upregulation (Figure 3C and Figure S3). Specifically, RNAi against *bli-1* or *mup-4* caused reduced MUP-4 staining in the CeHD area, which most likely accounted for the dramatic upregulation of AMPs (Figure 3C and Figures S3B and S3C). Loss of *ifb-1* or *vab-10a* slightly disturbed MUP-4 striped patterns at CeHDs, in accordance with the mild increase in *nlp-29* expression (Figure 3C and Figures S3E and S3F). Most other treatments did not interfere with MUP-4 localization, and as a result, no apparent AMP upregulation was detected (Figure 3C and Figure S3K). Taken together, these data support the notion that the transmembrane CeHD component MUP-4 at the apical side of the epidermis is crucial for relaying damage-induced immune response.

CeHD-Induced Immune Response Requires a STAT Protein, but Not Other Known AMP-Regulating Molecules

To determine the signaling pathway through which apical CeHDs drive AMP production, we examined players known to be required for epidermal AMP induction upon external insults such as fungal infection, physical injury, and hyperosmotic stress (Chisholm and Xu, 2012). Our analysis included Gα protein GPA-12, the toll-interleukin-like adaptor TIR-1, SEK-1 and PMK-1 of the p38-MAPK signaling cassette, the neuron-derived TGF-β homolog DBL-1 and its epidermal receptor SMA-6, the WNK-type protein kinase WNK-1, the GATA transcription factor

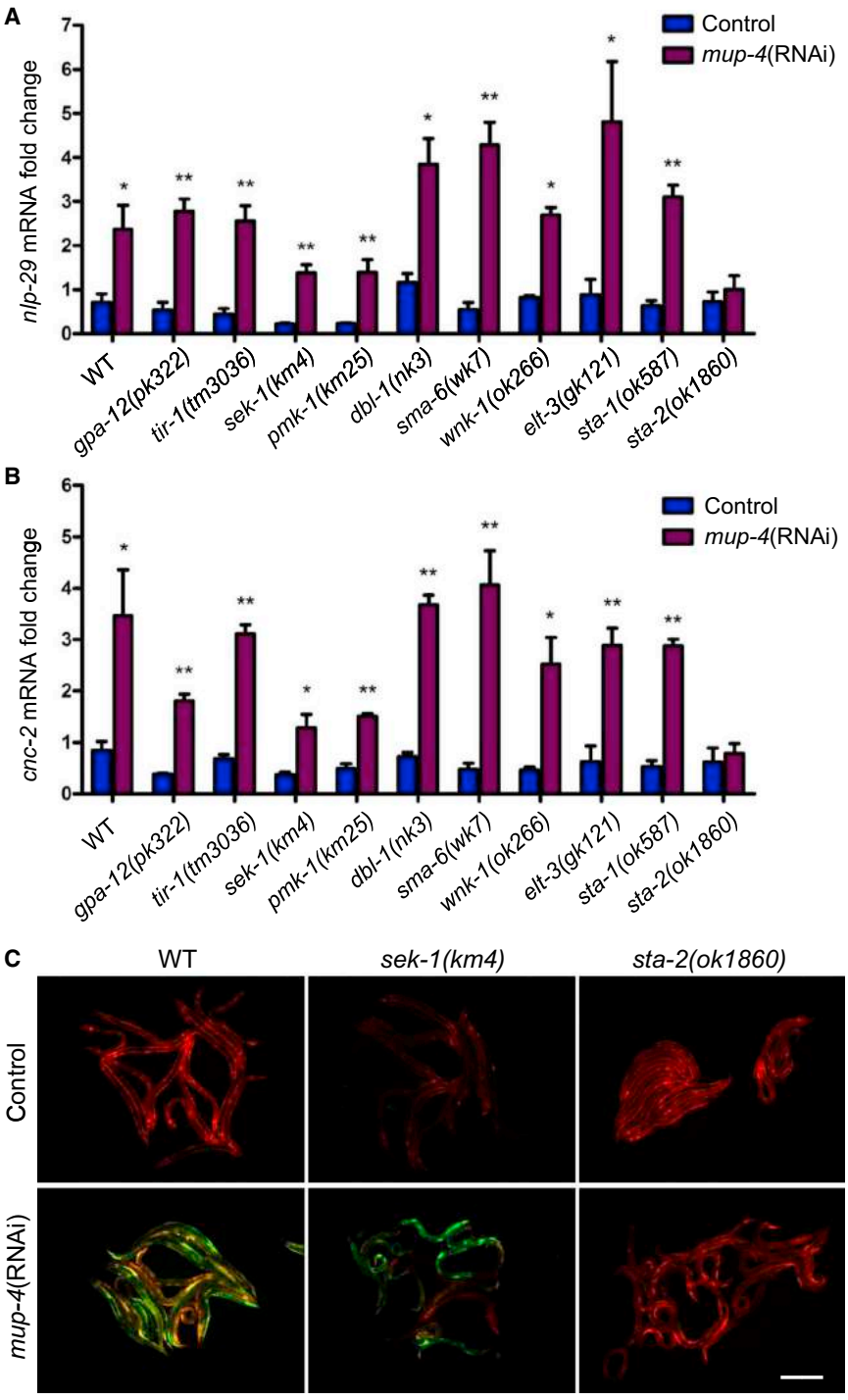

Figure 4. Induction of AMP Transcription by *mup-4* Inactivation Requires the STAT Family Protein STA-2

(A and B) Quantitative RT-PCR results show *nlp-29* or *cnc-2* expression after *mup-4* RNAi treatment in the wild-type control and loss-of-function mutants of *gpa-12*, *tir-1*, *sek-1*, *pmk-1*, *dbl-1*, *sma-6*, *wnk-1*, *elt-3*, *sta-1*, and *sta-2*. Error bars represent the mean ± SEM (three biological replicates, n ≥ 100/condition). Asterisks denote a significant increase in AMP expression in comparison to the control (*$p < 0.05$, **$p < 0.01$).

(C) Fluorescence images show the expression of Pnlp-29::GFP after *mup-4* RNAi treatment in the wild-type control and *sta-2(ok1860)* and *sek-1(km4)* mutants. Pcol-12::DsRed served as an internal control. The scale bar represents 300 μm.

ELT-3, and the two *C. elegans* STAT proteins STA-1 and STA-2 (Couillault et al., 2004; Lee et al., 2010; Pujol et al., 2008a; Ziegler et al., 2009; Zugasti and Ewbank, 2009). qPCR analysis showed that the functional loss of most of these pathways or players, with the exception of STA-2, did not block *nlp-29* or *cnc-2* upregulation caused by *mup-4* inactivation (Figures 4A and 4B). STA-2 function was previously shown to be necessary for the induction of AMPs by fungal infection or physical injury (Dierking et al., 2011). Here, we found that STA-2 inactivation abolished the elevation of *nlp-29* and *cnc-2* transcription caused by apical CeHD disassembly (Figures 4A and 4B). The observations obtained from Pnlp-29::GFP transgenic worms treated with *mup-4* RNAi are consistent with the qPCR results (Figure 4C). These data suggest that the immune response triggered by apical CeHD disruption does not require known immune signaling pathways in the epidermis but is directly mediated by STA-2.

STA-2 Is Localized to CeHD Attachment Structures at the Apical Membrane

The fact that apical CeHDs regulate AMP expression through STA-2 but not other signaling molecules suggests that CeHDs associate with STA-2. We next looked into the spatial relationship between STA-2 and CeHDs. Transgene-driven STA-2 fused to fluorescent proteins was previously shown to localize in the nucleus, in bands under the cuticle, and in endocytic vesicles of the epidermis (Dierking et al., 2011). To examine the subcellular localization of endogenous STA-2 in detail, we generated a STA-2 antibody recognizing peptides flanking its C-terminal SH2 domain. Immunostaining against STA-2 revealed that most endogenous STA-2 was distributed in a characteristic CeHD-like pattern in the epidermis of the healthy worms (solid arrow in Figure 5A and Figure S4E). Double labeling with CeHD marker MH4 showed that the stripes of STA-2 co-localized with those of the CeHDs (upper panel in Figure 5A). The mCherry::STA-2 fusion protein displayed similar localization patterns and was also present in CeHDs from the embryonic stage (arrows in Figure S4A, S4B, and S4D). By expressing STA-2 in the pharyngeal epithelium, whose apical and basal membranes are much further apart, we could distinguish an

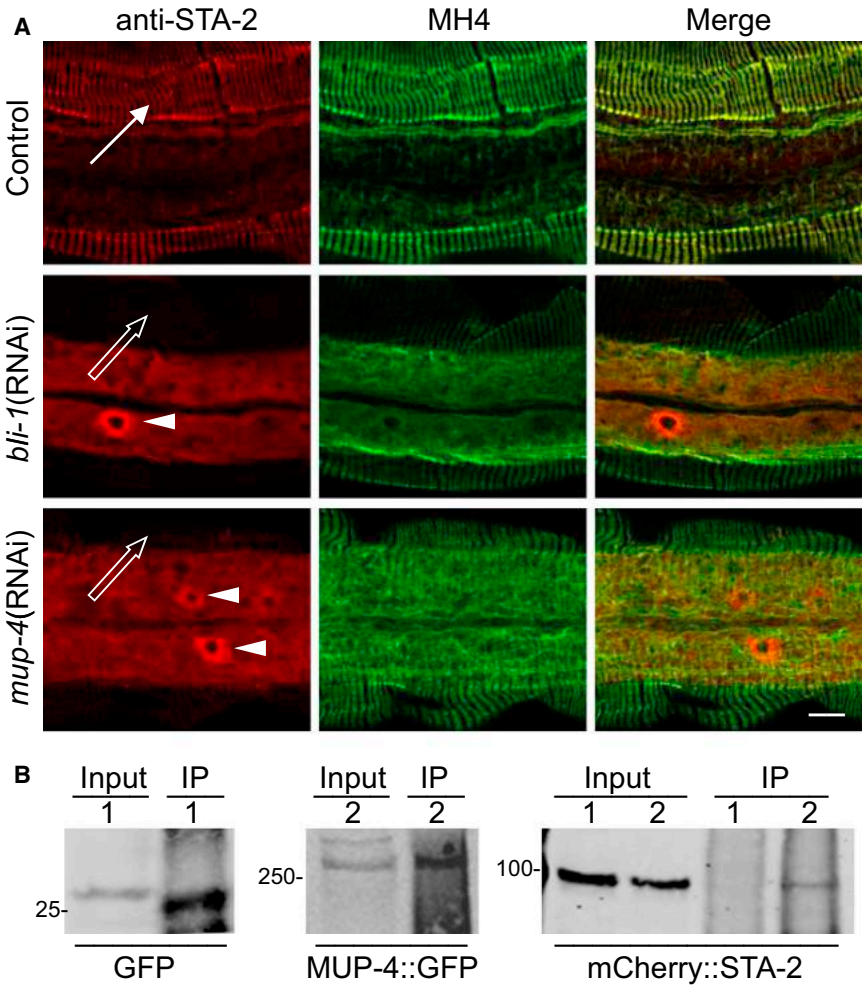

Figure 5. CeHDs Regulate AMP Expression through Association with STA-2

(A) Immunostaining of CeHD marker MH4 (green) and STA-2 (red) in the intact epidermis or epidermis damaged by *bli-1* or *mup-4* RNAi treatment. The solid arrow points to CeHDs. Outlined arrows point to the loss of STA-2 localization in the CeHDs. Arrowheads point to the nuclei. The scale bar represents 10 μm.

(B) Co-IP of MUP-4 and STA-2 was performed by co-expression of MUP-4::GFP and mCherry::STA-2 (2) or of control GFP and mCherry::STA-2 (1) in the *C. elegans* epidermis and subsequent immunoprecipitation using anti-GFP beads. Immunoblotting was performed on total worm lysates (input) and immunoprecipitates (IP) with the use of anti-GFP and anti-mCherry antibodies.

See also Figure S4.

apical enrichment of STA-2 (open arrowhead in Figure S4C). These observations indicate that most endogenous STA-2 molecules are tethered to CeHDs at the apical membrane of the intact epidermis.

The data suggest that MUP-4 is the main molecule tethering STA-2 to CeHDs. To test whether STA-2 forms a protein complex with MUP-4, we performed co-immunoprecipitation (co-IP) in *C. elegans* by immunoprecipitation of GFP-tagged full-length MUP-4 receptor or negative control GFP alone and subsequent immunoblotting against mCherry-tagged STA-2 expressed in the epidermis (Figure 5B). STA-2 could be co-immunoprecipitated together with full-length MUP-4, suggesting that these two proteins belong to the same protein complex in the *C. elegans* epidermis.

We next asked whether there is a correlation between the amount of CeHD-associated STA-2 and the amount of AMP transcription. We examined STA-2 localization after inactivation of *bli-1* or *mup-4*, the two robust inducers of *nlp-29* and *cnc-2* (Figure 2 and Figure S2). Consistent with our hypothesis, RNAi against *bli-1* or *mup-4* resulted in significantly decreased STA-2 localization at the CeHDs (open arrows in Figure 5A). In addition, STA-2 staining was increased in both the cytoplasmic region outside of the CeHDs and in the epidermal nuclei (arrowheads in Figure 5A). Taken together, these results suggest that the physical association between STA-2 and apical CeHDs suppresses the ability of STA-2 to induce AMP production in the epidermis.

Extensive Injury Bypasses p38-MAPK Signaling and Directly Activates STA-2 to Drive AMP Expression

We reasoned that the physiological purpose of STA-2 attachment to CeHDs might be to enable a quick and direct defense response against structural insults without going through multiple steps of signaling transduction. To test this hypothesis, we employed a severe epidermal-injury approach by using micrometer-scale fine glass shards, which allowed us to introduce multiple wounds in the epidermis of a single worm (Figure 6A and Figure S5). It was previously shown that a single epidermal wound induced *nlp-29* expression via a process requiring function of both the p38-MAPK pathway and STA-2 and that STA-2 might act downstream of p38-MAPK signaling (Dierking et al., 2011; Pujol et al., 2008a). In agreement, mild epidermal injury caused by a microinjection needle puncture (one wound per animal) triggered *nlp-29* upregulation in a p38- and STA-2-dependent manner, as shown by Pnlp-29::GFP induction in wild-type worms, but not in *sek-1(km4)* or *sta-2(ok1860)* mutants (Figure 6B). However, when multiple wounds were generated, *sek-1(km4)* mutants were capable of expressing as much *nlp-29* as wild-type worms were, suggesting that the induction of *nlp-29* was no longer dependent on the p38-MAPK pathway. In contrast, severe wounding showed dependency on STA-2 function and therefore did not increase *nlp-29* expression in *sta-2(ok1860)* mutants (Figure 6B). The quantification results of qPCR analysis are consistent with the observations obtained from the Pnlp-29::GFP reporter (Figures 6C and 6D). The results demonstrate that similar to the immune response triggered by CeHD disruption, severe epidermal injury could bypass conventional immune pathways and directly turn on STA-2 activity.

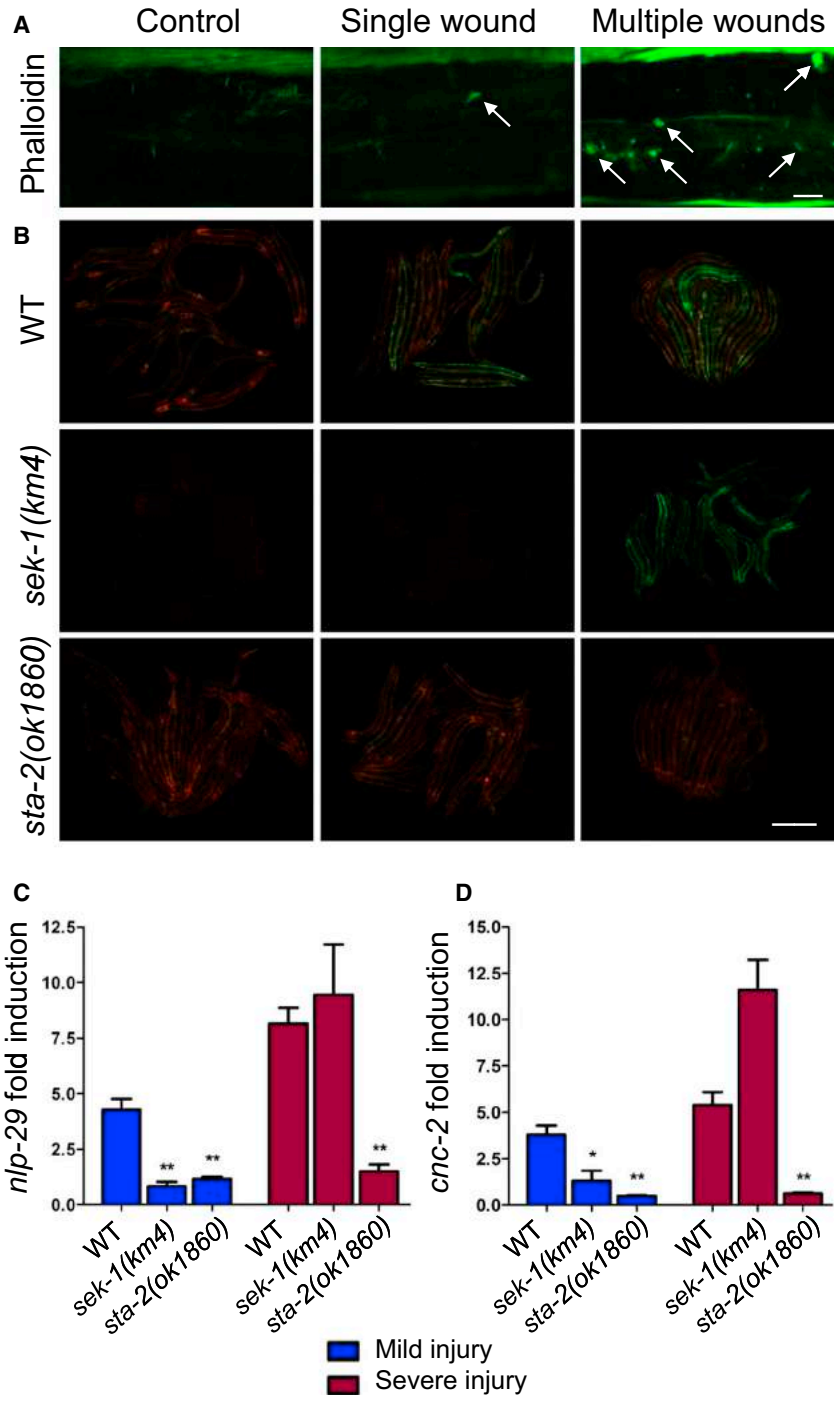

Figure 6. Extensive Wounding in the Epidermis Bypasses the p38-MAPK Pathway and Directly Upregulates *nlp-29* in a STA-2-Dependent Manner

(A) Phalloidin staining of worms subjected to needle wounding (single wound) or extensive wounding (multiple wounds). The wounds in the epidermis are marked by phalloidin-stained actin foci surrounding each healing wound (arrows). The scale bar represents 10 μm.

(B) Expression of Pnlp-29::GFP after introduction of a single wound or multiple wounds in the epidermis of wild-type worms, *sek-1(km4)* mutants deficient in p38-MAPK signaling, or STA-2-loss-of-function mutant *sta-2(ok1860)*. The scale bar represents 300 μm.

(C and D) Quantitative RT-PCR results show *nlp-29* or *cnc-2* expression after mild (single wound) or severe (multiple wounds) injury in the wild-type control and *sek-1(km4)* and *sta-2(ok1860)* mutants. Error bars represent the mean ± SEM (three biological replicates, n ≥ 100/condition). Asterisks denote a significant decrease in AMP upregulation in comparison to the control (*$p < 0.05$, **$p < 0.01$).

See also Figure S5.

Hemidesmosome Disassembly Induces AMP Expression in Primary Human Epidermal Keratinocytes

The results obtained from the *C. elegans* skin model suggest that the hemidesmosomes are crucial for immune surveillance through structural damage in the epidermis. To test whether a similar phenomenon exists in the mammalian epidermal cells, we utilized a primary adult human epidermal keratinocyte (HEKa) culture and examined the involvement of its major supporting structures in immune-response activation. These structures include actin, microtubule and keratin cytoskeletons, and keratin-linked hemidesmosomes protein complexes (HPCs) and actin-linked focal contacts (FCs), the two attachment structures responsible for anchoring HEK cells on the culture surface (Tsuruta et al., 2011). We first disrupted the aforementioned structural components individually by antibody blocking, small interfering RNA (siRNA) knockdown, or drug treatment (Ozawa et al., 2010). Specifically, actin and microtubule cytoskeletons were disrupted by cytochalasin D and nocodazole treatment, respectively. The synthesis of keratins 5 and 14, the intermediate filament proteins anchoring to the HPCs, was blocked by siRNA knockdown (Zhang and Labouesse, 2010). HPC assembly was inhibited by function-blocking antibodies against their transmembrane receptors α6-integrin (GoH3) or β4-integrin (3E1), and FC assembly was inhibited by a blocking antibody against α3-integrin (P1B5). The efficiency of structural disruption was confirmed by immunostaining (Figure S6).

We next quantified the expression of several key innate immune effectors produced by skin keratinocytes after disruption of each structure (Di Meglio et al., 2011; Nestle et al., 2009). These effectors included cationic AMPs (β-defensins and cathelicidin) and cytokines interleukin-6 (IL-6), IL-8, and tumor necrosis factor α (TNF-α). Consistent with findings from the *C. elegans* epidermis model, collapse of actin or microtubule cytoskeletons in HEKa cells did not affect the immune effectors tested (Figure 7A). Disassembly of cell-matrix junctions of HPCs or FCs, on the other hand, triggered robust and specific transcription

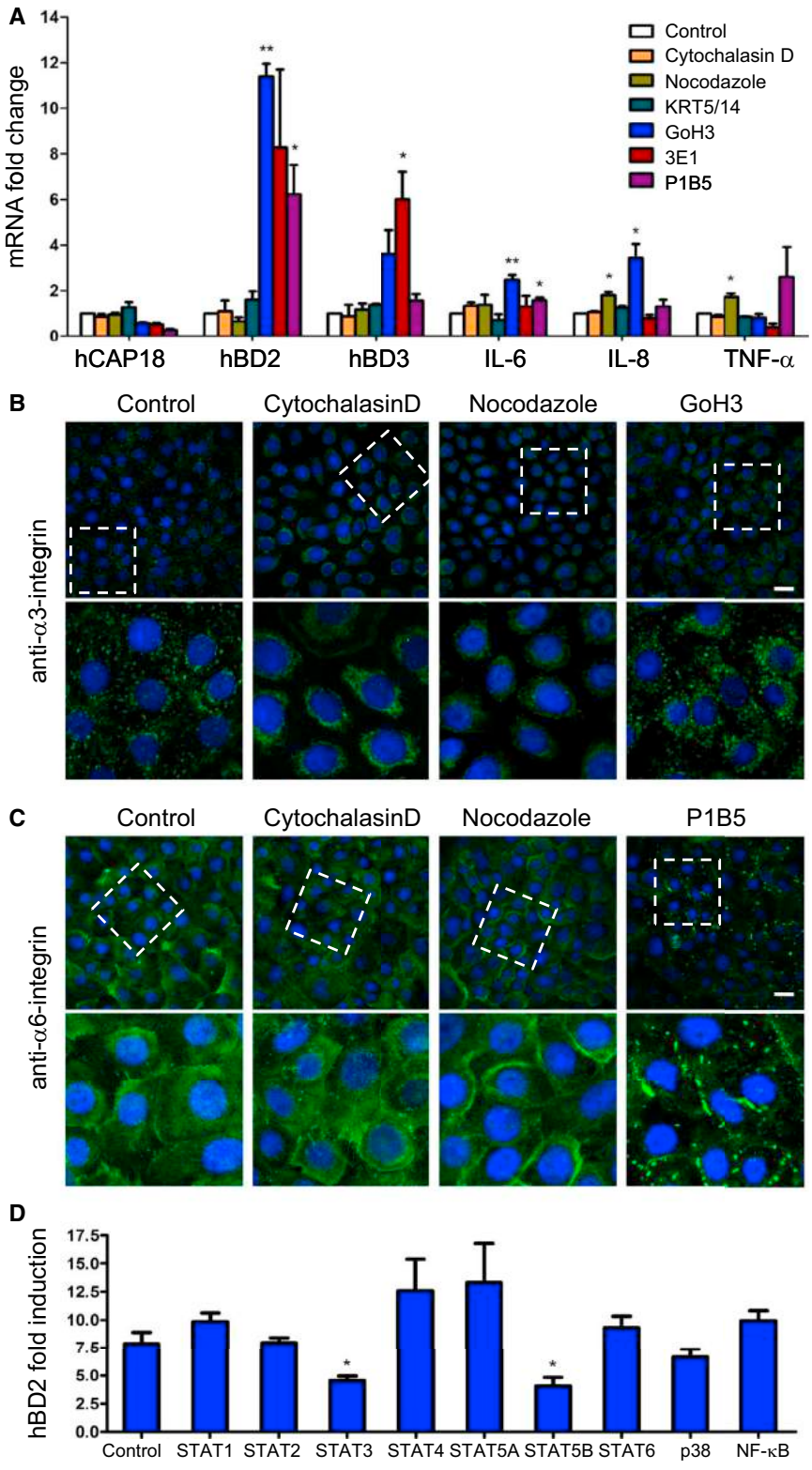

Figure 7. Disruption of the Hemidesmosome Protein Complexes Induces AMP Expression in Primary HEKa Cells

(A) Quantitative RT-PCR results show cathelicidin (hCAP18), β-defensins (hBD2 and hBD3), IL-6, IL-8, and TNF-α expression in primary HEKa cells after disruption of actin cytoskeleton (cytochalasin D), microtubule bundles (nocodazole), intermediate filaments (*KRT5* and *KRT14* siRNA), focal contacts (anti-α3-integrin P1B5 antibody blocking), or hemidesmosomes (anti-α6-integrin GoH3 or anti-β4-integrin 3E1 antibody blocking). Error bars represent the mean ± SEM (three biological replicates). Asterisks denote a significant increase in gene expression in comparison to the control (*$p < 0.05$, **$p < 0.01$).

(B) Representative confocal images of focal contacts labeled by anti-α3-integrin immunostaining in HEKa cells with damaged actin cytoskeleton (cytochalasin D), microtubule bundles (nocodazole), or hemidesmosomes (GoH3). The scale bar represents 20 μm.

(C) Representative confocal images of hemidesmosomes labeled by anti-α6-integrin immunostaining in HEKa cells with damaged actin cytoskeleton (cytochalasin D), microtubule bundles (nocodazole), or focal contacts (P1B5). The scale bar represents 20 μm.

(D) Quantitative RT-PCR results show β-defensin induction in response to anti-α6-integrin treatment after siRNA knockdown of each STAT protein or inhibition of p38-MAPK or NF-κB activity. Error bars represent the mean ± SEM (three biological replicates). An asterisk denotes a significant decrease in β-defensin induction in comparison to the control (*$p < 0.05$).

See also Figure S6.

of β-defensins, but not transcription of cathelicidin. IL-6 and IL-8 expression also increased moderately upon disassembly of HPCs, but not to the same extent as β-defensin upregulation (Figure 7A). The fact that the AMPs were upregulated to a greater extent than cytokines suggests that this immune-activating process might originate from a rather primitive stage during evolution.

Previous reports have demonstrated that HPCs, FCs, and cytoskeletons show complex interactions and that the disturbance of one structure could affect the organization of another in cultured cells (Ozawa et al., 2010). Therefore, to clarify which type of attachment is the primary trigger for AMP production, we examined the organization of HPCs and FCs after targeted disruption of different structures by immunostaining. FCs were disrupted not only by α3-integrin blocking but also by depolymerization of actin or microtubule cytoskeletons. Indeed, the number of α3-integrin-positive foci was reduced after treatment with cytochalasin D or nocodazole, yet such reduction did not increase AMP or cytokine levels (Figures 7A and 7B). In contrast, cells treated with α6-integrin antibody possessed intact FC attachments, although AMP expression was upregulated in these cells

(Figures 7A and 7B). Therefore, we conclude that upregulation of β-defensin 2 by α3-integrin antibody blocking is irrelevant to the disassembled FCs. Furthermore, immunostaining against α6-integrin showed that the organization of HPC attachments was also affected by an α3-integrin blocking antibody (Figure 7C). Thus, induction of β-defensin transcription correlated with disrupted HPCs but was independent of FC disorganization. This suggests that the HPCs, but not the more dynamic FCs, are the main attachment structures capable of inducing an innate immune response in damaged HEKa cells.

We next investigated the involvement of all seven human STAT transcription factors (STAT1, STAT2, STAT3, STAT4, STAT5a, STAT5b, and STAT6) in HD-mediated immune activation in HEKa cells. STAT proteins were inhibited by siRNA knockdown (Figure S6E). In addition, inhibitors of p38-MAPK and NF-κB were also tested because these signaling pathways are common inducers of epidermal β-defensins (Di Meglio et al., 2011; Nestle et al., 2009). The induction of β-defensin by HPC disassembly was analyzed by qPCR in STAT-, p38-, or NF-κB-inactivated cells. The results in Figure 7D show that among the seven STATs, inactivation of STAT3 or STAT5B attenuated AMP upregulation after HPC disassembly in HEKa cells. Neither p38-MAPK nor NF-κB was required for the induction of β-defensin (Figure 7D). These observations are consistent with data from the *C. elegans* model, in which the STAT5B homolog STA-2 but not the p38 MAPK pathway was required for the induction of AMPs after epidermal damage.

DISCUSSION

In conclusion, we propose that *C. elegans* hemidesmosomes serve as docking sites for STA-2 molecules at the apical membrane and restrict STA-2 activity under normal conditions. When the epidermis is subjected to internal or external insults that disintegrate the apical CeHDs, it loses the restriction upon STA-2 function and eventually activates AMP transcription. This mechanism unravels a unique danger-sensing machinery that does not involve extracellular signaling molecules or complicated signaling pathways. Instead, the epidermal innate immune system possesses a cell-autonomous surveillance program installed within its stable adhesion structures. This immune-regulating mechanism might represent an ancient backup strategy for danger sensing and self-defense in the epidermis of multi-cellular organisms. In the natural environment, such a straightforward strategy enables the epidermis to better prepare for the inevitable pathogen invasion upon barrier breach. It also offers a second line of defense against external insults if the classic immune-activating pathways are compromised.

In higher organisms with more sophisticated immune systems, a remnant of such simple defense machinery in the epidermal architecture is less necessary but could trigger unwanted immune responses if the structures are damaged by non-infectious causes. Indeed, internal disturbance of epidermal structural components is often associated with the onset of skin inflammation. For example, ablation of hemidesmosome components in mouse skin leads to upregulation of pro-inflammatory cytokines in the epidermis and infiltration of immune cells (Niculescu et al., 2011). Skin keratinocytes lacking keratin 16 are more vulnerable to over-activated inflammatory response (Lessard et al., 2013). Genetic mutations of human IF-associated protein filaggrin, which is homologous to the cytoplasmic domain of *C. elegans* MUP-4, have been identified as causes of skin-inflammatory diseases such as atopic eczema (Sandilands et al., 2009). Most current studies tend to attribute the link between epidermal structural damage and inflammation to the compromised physical-barrier function and subsequent infiltration of pathogens or allergens. However, our discoveries from the *C. elegans* epidermis and primary HEK cells propose a more central role of the epidermal cells in triggering inflammatory response. They might help clarify the contribution of epidermal damage in the initiation and augmentation of certain inflammatory diseases. Our findings also carry potential implications for pathological circumstances in which other types of epithelial tissues are damaged, especially in hemidesmosome-containing tissues such as the airway and intestinal epithelia.

The primary function of the apical CeHD receptor MUP-4 is thought to provide mechanical attachment for the *C. elegans* epidermis. However, it is worth noting that MUP-4 is a large 2,107-aa protein with complex functional domains. The extracellular portion of MUP-4 contains 27 epidermal growth factor (EGF) repeats, a class B1 EGF-notch motif, a von Willebrand factor A domain for collagen binding, and two sea urchin enterokinase modules for glycosylated proteins (Hong et al., 2001). These functional domains endow MUP-4 with potential capabilities to receive and interpret complex extracellular signals. Therefore, it is possible that MUP-4 could serve as a regulator of epidermal immune response by receiving external signals in the intact epidermis. It was recently revealed that the G-protein-coupled receptor DCAR-1 recognizes an endogenous metabolite and regulates injury-induced innate defense in the epidermis via the p38-MAPK signaling pathway (Zugasti et al., 2014). Although the CeHD-mediated immune response is independent of the p38-MAPK pathway during severe epidermal damage, it would be interesting to evaluate the interaction between MUP-4 and DCAR-1 in the intact epidermis.

Unlike mammalian STAT proteins, which often remain latent in the cytosol until activated, the *C. elegans* STA-2 molecules were found to be mostly tethered to the CeHDs in the unchallenged epidermis. Therefore, it is reasonable to presume that the physical interaction between MUP-4 and STA-2 is crucial for the regulation of STA-2 activity. However, the exact chain of events that take place after STA-2's detachment from CeHDs remains a mystery. The DNA-binding domain of human STAT5B has much less homology with STA-2 than with STA-1 (Dierking et al., 2011). Therefore, the DNA-binding and transcription-activation functions of STA-2 in the nucleus still await further testing. It also remains to be determined whether STA-2 could serve as an activator of additional signaling pathways while being released into the cytosol upon epidermal damage.

To summarize, our discoveries not only provide a comprehensive image of epidermal innate immune response upon structural damage but also reveal important roles of stable adhesions such as hemidesmosomes in regulating innate immunity. Our results obtained from HEKa cultures suggest that HPCs, but not the dynamically regulated FCs, specifically control the expression of immune effectors. It is intriguing that the epidermal cells

should choose the stable adhesion complexes but not their other structural entities to perform immune-regulating roles. One reason could be that these structures are less likely to be disturbed during normal biological processes. Another possible reason could lie in their unique ways of connecting tissues both mechanically and biochemically. Our previous studies have demonstrated that *C. elegans* hemidesmosomes are endowed with the potential to convert contractile force into biochemical signaling during epidermal morphogenesis (Zhang et al., 2011). It is reasonable to presume that such mechano-sensing properties of the hemidesmosomes can also be incorporated into their immune surveillance functions with cooperation from immune regulators coupled to these adhesion structures.

EXPERIMENTAL PROCEDURES

Worm Strains and Genetic Methods

C. elegans strains were maintained at 20°C as previously described (Brenner, 1974). The strains used in this study were mostly obtained from the Caenorhabditis Genetics Center, which is funded by the NIH Office of Research Infrastructure Programs (P40 OD010440).

Worm RNAi and Drug Treatment

RNAi of *C. elegans* was induced by bacterial feeding as previously described (Kamath et al., 2003). For disruption of microtubule bundles, L4-stage wild-type worms were soaked in 60 μg/ml nocodazole dissolved in M9 buffer for 2 hr and then recovered in M9 for 2 hr before collection. Control groups were soaked in M9 buffer for 4 hr before analysis.

Molecular Biology and Transgenesis

Constructs used in this study were generated with the ClonExpress TM One Step Cloning Kit (Vazyme Biotech). All fragments obtained by PCR amplification were confirmed by sequencing for confirmation of mutations. Microinjection and transgenesis were carried out as previously described (Zhang et al., 2011).

Immunostaining and Fluorescence Microscopy of *C. elegans*

Worms were fixed and stained by indirect immunofluorescence as previously described (Costa et al., 1997). 12A6, AA4.3, and MH monoclonal antibodies were purchased from the Developmental Studies Hybridoma Bank (University of Iowa). The MUP-4 polyclonal antibody was raised against peptide PRAKLARPLYGDEMGDD as previously described (Hong et al., 2001). The STA-2 polyclonal antibody was raised against peptides CRNLAPDEIYFDNQGAAT and CVAEEFQHKKSASAEGDW, flanking the SH2 domain of STA-2. Phalloidin staining of the epidermal actin filaments was performed as previously described (Costa et al., 1997). Single-plane fluorescent images were captured with the Nikon A1 confocal microscope or Leica TCS SP5 confocal microscope and processed with ImageJ (http://rsb.info.nih.gov/ij/).

Co-IP with Worm Lysates

The transgenic strains carrying Pdpy-7::mCherry::STA-2 and MUP-4::GFP or Pdpy-7::mCherry::STA-2 and GFP alone were used for studying the interaction between STA-2 and MUP-4. The co-IP experiment was performed with whole worm lysates according to the protocol kindly provided by Mengqiu Dong's lab (National Institute of Biological Sciences, Beijing). Detailed procedures of co-IP are provided in the Supplemental Experimental Procedures.

Quantitative RT-PCR Analysis

For quantitative RT-PCR analysis, total RNA was extracted by the RNAiso Plus reagent (TakaRa) and reverse transcribed by PrimeScript RT Master Mix (TakaRa). Real-time PCR was performed with FastStart Universal SYBR Green Master (Roche) on Mastercycler ep realplex (Eppendorf). Each experiment was repeated at least three times with cDNA templates derived from different RNA samples, and each reaction was run in quadruplicate. Normalized against the reference gene *act-1*, the expression levels of target genes relative to controls were calculated with REST 2009 software (QIAGEN). Statistical analysis was performed with a Student's t test with Prism 5.0 software (GraphPad Software). Significance was accepted for $p < 0.05$.

Physical Injury of the Epidermis

For an assay of severe physical injury, worms were placed on a layer of fine glass shards. Specifically, 0.25-mm-thick glass capillaries (BF-100-50-10, Sutter) were ground to produce glass shards with diameters ranging from 10 to 100 μm. Glass shards were then washed with and stored in 75% ethanol in a 15-ml conical tube until use. Over- or under-sized shards were removed by gravity separation and a pass through a 300 mesh filter sieve. The length of the longest axis for each glass particle was measured and analyzed by ImageJ. For preparation of nematode growth medium (NGM) plates for injury, glass shards were spread evenly onto the plate until they covered the entire agar surface. A chunk of NGM agar with hundreds of worms was then placed upside down onto the glass shards, gently pressed, and left untouched for 5 min before the worms were moved to new plates for recovery. This method does not cause significant lethality among treated worms. Injured worms were then transferred to fresh plates with OP50 and collected 1 hr later for phalloidin staining or 5 hr later for GFP imaging.

Primary HEKa Culture and Treatments

The normal HEKa (FC-0025) cell line was purchased from Lifeline Cell Technology and maintained under the manufacturer's protocol.

For drug treatment, 80% confluent HEKa cells were treated with 200 nM cytochalasin D, 2 μM nocodazole, or DMSO control for 3 hr before gene-expression analysis or immunostaining. For p38 and NF-κB inactivation, cells were treated with 1 μM SB203580 or 10 μM BAY11-7082 for 24 hr before analysis. For functional blocking of integrins, cells were treated with 50 μg/ml blocking antibodies for 24 hr before analysis. For siRNA knockdown, transfections were performed with 100 nm siRNA and Lipofectamine 3000 (L3000-015) from Life Technologies. Transfection mixtures were replaced by DermaLife medium after 24 hr and incubated for an additional 24 hr before being assayed for gene expression. For all gene-expression analyses, the mRNA levels of each experimental group were compared to its own control group with mock treatment. The baseline gene-expression levels of all control groups were normalized as 1.

SUPPLEMENTAL INFORMATION

Supplemental Information includes six figures and Supplemental Experimental Procedures and can be found with this article online at http://dx.doi.org/10.1016/j.immuni.2015.01.014.

AUTHOR CONTRIBUTIONS

H.Z. and S.X. designed the study. Y. Zhang performed most experiments. Y. Zhang and H.Z. analyzed data. W.L. helped with most experiments. L.L. prepared samples for gene-expression analysis and constructed plasmids. Y.L. helped with RNAi, transgenesis, and immunostaining. R.F. performed antibody testing and perfected immunostaining conditions. Y. Zhu helped with severe injury approach and provided technical assistance. J.L. helped with co-IP experiments. Y. Zhou contributed to confocal imaging tasks. Y. Zhang and H.Z. wrote the manuscript.

ACKNOWLEDGMENTS

We are grateful to Michel Labouesse, Hong Zhang, Xiaochen Wang, Shiqing Cai, the Caenorhabditis Genetics Center, and NBP-Japan for reagents, as well as Shuai Wang, Ming Zhu, Yiling Zhang, and Yanmei Li for technical support. We thank Min Han for discussion and members of the H.Z. lab (He Wang, Xiaoran Dong, Lin Sun, and Qin Wang) for help with the manuscript. This work was supported by grants from Major State Basic Research Development Program of China (2013CB530501), National Natural Science Foundation of China (31271429 and 31471265), Jiangsu Provincial Innovative Research Team, the Program for Changjiang Scholars and Innovative Research Team in University, and the Priority Academic Development Program of Jiangsu Province Higher Education Institutions.

Received: October 17, 2014
Revised: December 29, 2014
Accepted: January 6, 2015
Published: February 17, 2015

REFERENCES

Bercher, M., Wahl, J., Vogel, B.E., Lu, C., Hedgecock, E.M., Hall, D.H., and Plenefisch, J.D. (2001). mua-3, a gene required for mechanical tissue integrity in Caenorhabditis elegans, encodes a novel transmembrane protein of epithelial attachment complexes. J. Cell Biol. *154*, 415–426.

Bosher, J.M., Hahn, B.S., Legouis, R., Sookhareea, S., Weimer, R.M., Gansmuller, A., Chisholm, A.D., Rose, A.M., Bessereau, J.L., and Labouesse, M. (2003). The Caenorhabditis elegans vab-10 spectraplakin isoforms protect the epidermis against internal and external forces. J. Cell Biol. *161*, 757–768.

Brenner, S. (1974). The genetics of Caenorhabditis elegans. Genetics *77*, 71–94.

Chisholm, A.D., and Xu, S. (2012). The Caenorhabditis elegans epidermis as a model skin. II: differentiation and physiological roles. Wiley interdisciplinary reviews. Dev. Biol. *1*, 879–902.

Costa, M., Draper, B.W., and Priess, J.R. (1997). The role of actin filaments in patterning the Caenorhabditis elegans cuticle. Dev. Biol. *184*, 373–384.

Couillault, C., Pujol, N., Reboul, J., Sabatier, L., Guichou, J.F., Kohara, Y., and Ewbank, J.J. (2004). TLR-independent control of innate immunity in Caenorhabditis elegans by the TIR domain adaptor protein TIR-1, an ortholog of human SARM. Nat. Immunol. *5*, 488–494.

Davis, M.M., and Engström, Y. (2012). Immune response in the barrier epithelia: lessons from the fruit fly Drosophila melanogaster. J. Innate Immun. *4*, 273–283.

De Gregorio, E., Han, S.J., Lee, W.J., Baek, M.J., Osaki, T., Kawabata, S., Lee, B.L., Iwanaga, S., Lemaitre, B., and Brey, P.T. (2002). An immune-responsive Serpin regulates the melanization cascade in Drosophila. Dev. Cell *3*, 581–592.

Di Meglio, P., Perera, G.K., and Nestle, F.O. (2011). The multitasking organ: recent insights into skin immune function. Immunity *35*, 857–869.

Dierking, K., Polanowska, J., Omi, S., Engelmann, I., Gut, M., Lembo, F., Ewbank, J.J., and Pujol, N. (2011). Unusual regulation of a STAT protein by an SLC6 family transporter in C. elegans epidermal innate immunity. Cell Host Microbe *9*, 425–435.

Ding, M., Goncharov, A., Jin, Y., and Chisholm, A.D. (2003). C. elegans ankyrin repeat protein VAB-19 is a component of epidermal attachment structures and is essential for epidermal morphogenesis. Development *130*, 5791–5801.

Gettner, S.N., Kenyon, C., and Reichardt, L.F. (1995). Characterization of beta pat-3 heterodimers, a family of essential integrin receptors in C. elegans. J. Cell Biol. *129*, 1127–1141.

Hong, L., Elbl, T., Ward, J., Franzini-Armstrong, C., Rybicka, K.K., Gatewood, B.K., Baillie, D.L., and Bucher, E.A. (2001). MUP-4 is a novel transmembrane protein with functions in epithelial cell adhesion in Caenorhabditis elegans. J. Cell Biol. *154*, 403–414.

Hresko, M.C., Schriefer, L.A., Shrimankar, P., and Waterston, R.H. (1999). Myotactin, a novel hypodermal protein involved in muscle-cell adhesion in Caenorhabditis elegans. J. Cell Biol. *146*, 659–672.

Kamath, R.S., Fraser, A.G., Dong, Y., Poulin, G., Durbin, R., Gotta, M., Kanapin, A., Le Bot, N., Moreno, S., Sohrmann, M., et al. (2003). Systematic functional analysis of the Caenorhabditis elegans genome using RNAi. Nature *421*, 231–237.

Lee, K.Z., Kniazeva, M., Han, M., Pujol, N., and Ewbank, J.J. (2010). The fatty acid synthase fasn-1 acts upstream of WNK and Ste20/GCK-VI kinases to modulate antimicrobial peptide expression in C. elegans epidermis. Virulence *1*, 113–122.

Lessard, J.C., Piña-Paz, S., Rotty, J.D., Hickerson, R.P., Kaspar, R.L., Balmain, A., and Coulombe, P.A. (2013). Keratin 16 regulates innate immunity in response to epidermal barrier breach. Proc. Natl. Acad. Sci. USA *110*, 19537–19542.

Lints, R., and Hall, D.H. (2009). The Cuticle. In Wormatlas. http://dx.doi.org/10.3908/wormatlas.1.12.

McKeown, C., Praitis, V., and Austin, J. (1998). sma-1 encodes a betaH-spectrin homolog required for Caenorhabditis elegans morphogenesis. Development *125*, 2087–2098.

McMahon, L., Muriel, J.M., Roberts, B., Quinn, M., and Johnstone, I.L. (2003). Two sets of interacting collagens form functionally distinct substructures within a Caenorhabditis elegans extracellular matrix. Mol. Biol. Cell *14*, 1366–1378.

Melo, J.A., and Ruvkun, G. (2012). Inactivation of conserved C. elegans genes engages pathogen- and xenobiotic-associated defenses. Cell *149*, 452–466.

Mullen, G.P., Rogalski, T.M., Bush, J.A., Gorji, P.R., and Moerman, D.G. (1999). Complex patterns of alternative splicing mediate the spatial and temporal distribution of perlecan/UNC-52 in Caenorhabditis elegans. Mol. Biol. Cell *10*, 3205–3221.

Nestle, F.O., Di Meglio, P., Qin, J.Z., and Nickoloff, B.J. (2009). Skin immune sentinels in health and disease. Nat. Rev. Immunol. *9*, 679–691.

Niculescu, C., Ganguli-Indra, G., Pfister, V., Dupé, V., Messaddeq, N., De Arcangelis, A., and Georges-Labouesse, E. (2011). Conditional ablation of integrin alpha-6 in mouse epidermis leads to skin fragility and inflammation. Eur. J. Cell Biol. *90*, 270–277.

Ozawa, T., Tsuruta, D., Jones, J.C., Ishii, M., Ikeda, K., Harada, T., Aoyama, Y., Kawada, A., and Kobayashi, H. (2010). Dynamic relationship of focal contacts and hemidesmosome protein complexes in live cells. J. Invest. Dermatol. *130*, 1624–1635.

Pasti, G., and Labouesse, M. (2014). Epithelial junctions, cytoskeleton, and polarity, WormBook, ed. (The *C. elegans* Research Community), http://dx.doi.org/10.1895/wormbook.1.56.2, http://www.wormbook.org.

Patterson, R.A., Juarez, M.T., Hermann, A., Sasik, R., Hardiman, G., and McGinnis, W. (2013). Serine proteolytic pathway activation reveals an expanded ensemble of wound response genes in Drosophila. PLoS ONE *8*, e61773.

Perez-Moreno, M., Davis, M.A., Wong, E., Pasolli, H.A., Reynolds, A.B., and Fuchs, E. (2006). p120-catenin mediates inflammatory responses in the skin. Cell *124*, 631–644.

Perez-Moreno, M., Song, W., Pasolli, H.A., Williams, S.E., and Fuchs, E. (2008). Loss of p120 catenin and links to mitotic alterations, inflammation, and skin cancer. Proc. Natl. Acad. Sci. USA *105*, 15399–15404.

Pujol, N., Cypowyj, S., Ziegler, K., Millet, A., Astrain, A., Goncharov, A., Jin, Y., Chisholm, A.D., and Ewbank, J.J. (2008a). Distinct innate immune responses to infection and wounding in the C. elegans epidermis. Curr. Biol. *18*, 481–489.

Pujol, N., Zugasti, O., Wong, D., Couillault, C., Kurz, C.L., Schulenburg, H., and Ewbank, J.J. (2008b). Anti-fungal innate immunity in C. elegans is enhanced by evolutionary diversification of antimicrobial peptides. PLoS Pathog. *4*, e1000105.

Rogalski, T.M., Mullen, G.P., Gilbert, M.M., Williams, B.D., and Moerman, D.G. (2000). The UNC-112 gene in Caenorhabditis elegans encodes a novel component of cell-matrix adhesion structures required for integrin localization in the muscle cell membrane. J. Cell Biol. *150*, 253–264.

Sandilands, A., Sutherland, C., Irvine, A.D., and McLean, W.H. (2009). Filaggrin in the frontline: role in skin barrier function and disease. J. Cell Sci. *122*, 1285–1294.

Sørensen, O.E., Thapa, D.R., Roupé, K.M., Valore, E.V., Sjöbring, U., Roberts, A.A., Schmidtchen, A., and Ganz, T. (2006). Injury-induced innate immune response in human skin mediated by transactivation of the epidermal growth factor receptor. J. Clin. Invest. *116*, 1878–1885.

Tsuruta, D., Hashimoto, T., Hamill, K.J., and Jones, J.C. (2011). Hemidesmosomes and focal contact proteins: functions and cross-talk in keratinocytes, bullous diseases and wound healing. J. Dermatol. Sci. *62*, 1–7.

Woo, W.M., Goncharov, A., Jin, Y., and Chisholm, A.D. (2004). Intermediate filaments are required for C. elegans epidermal elongation. Dev. Biol. *267*, 216–229.

Xu, S., and Chisholm, A.D. (2011). A Gαq-Ca^{2+} signaling pathway promotes actin-mediated epidermal wound closure in C. elegans. Curr. Biol. *21*, 1960–1967.

Zhang, H., and Labouesse, M. (2010). The making of hemidesmosome structures in vivo. Dev. Dyn. *239*, 1465–1476.

Zhang, H., Landmann, F., Zahreddine, H., Rodriguez, D., Koch, M., and Labouesse, M. (2011). A tension-induced mechanotransduction pathway promotes epithelial morphogenesis. Nature *471*, 99–103.

Ziegler, K., Kurz, C.L., Cypowyj, S., Couillault, C., Pophillat, M., Pujol, N., and Ewbank, J.J. (2009). Antifungal innate immunity in C. elegans: PKCdelta links G protein signaling and a conserved p38 MAPK cascade. Cell Host Microbe *5*, 341–352.

Zugasti, O., and Ewbank, J.J. (2009). Neuroimmune regulation of antimicrobial peptide expression by a noncanonical TGF-beta signaling pathway in Caenorhabditis elegans epidermis. Nat. Immunol. *10*, 249–256.

Zugasti, O., Bose, N., Squiban, B., Belougne, J., Kurz, C.L., Schroeder, F.C., Pujol, N., and Ewbank, J.J. (2014). Activation of a G protein-coupled receptor by its endogenous ligand triggers the innate immune response of Caenorhabditis elegans. Nat. Immunol. *15*, 833–838.

Immunity

Supplemental Information

Structural Damage in the *C. elegans* Epidermis Causes Release of STA-2 and Induction of an Innate Immune Response

Yun Zhang, Wenna Li, Linfeng Li, Yuanbao Li, Rong Fu, Yi Zhu, Jie Li, Yanfeng Zhou, Sidong Xiong, and Huimin Zhang

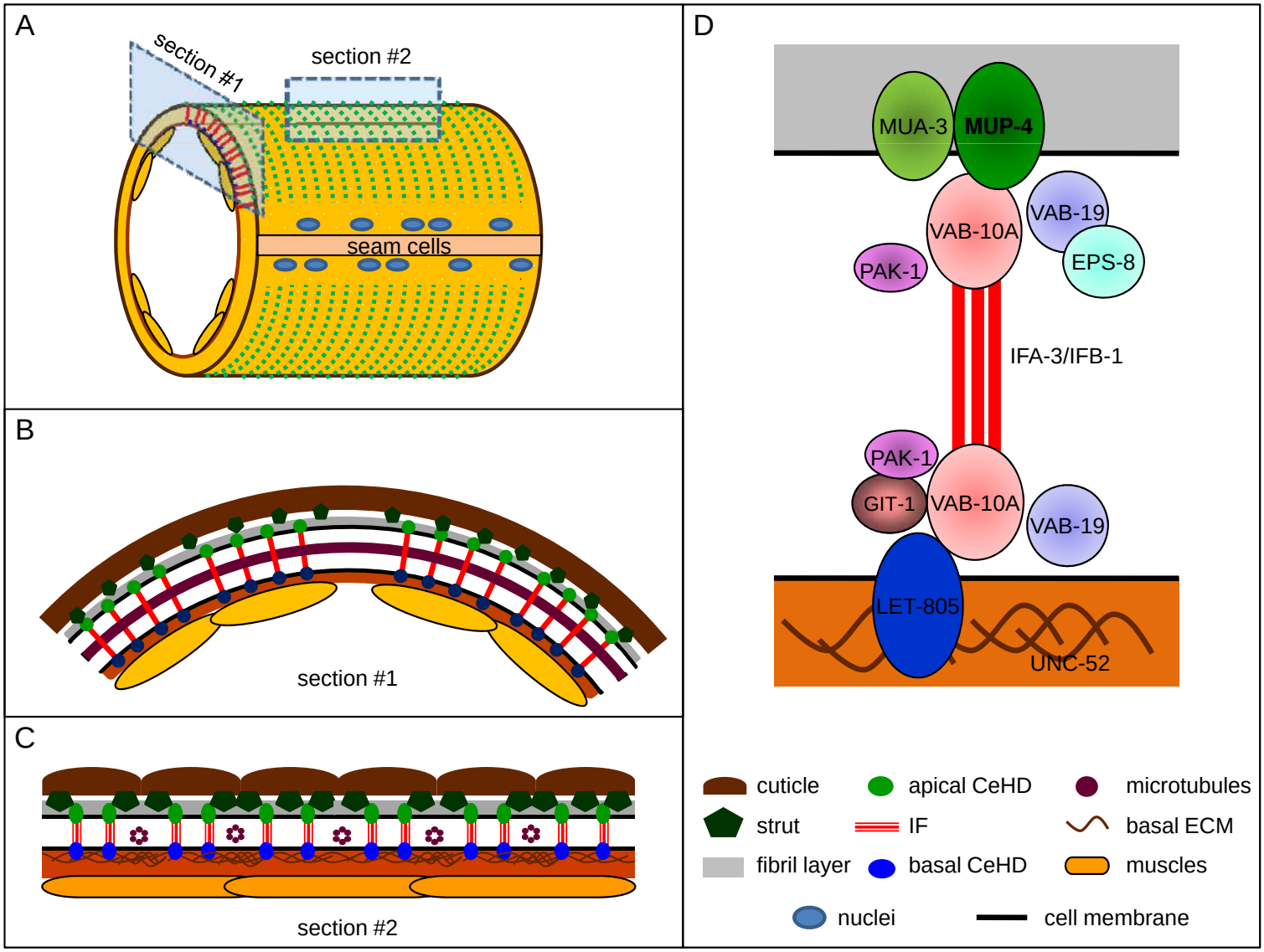

Figure S1: The architecture of adult *C. elegans* epidermis. Related to Figure 1

(A) Simplified body plan of the adult *C. elegans* epidermis at the mid-body region. Section 1 and 2 represents the position for cross or longitude section of the hyp7 epidermal cell，respectively. Dotted green lines represent apical CeHDs. **(B)** Relative positions of the epidermal supporting structures corresponding to the region in section #1. The thickness of the epidermis in this region is 100-300nm. The hyp7 epidermal cell is attached apically to the cuticle exoskeleton (brown) and basally to the muscle quadrants (yellow). The trans-epidermal CeHDs tether all three tissue layers together through the IFs (red). Microtubule bundles (purple) run across the epidermis and are positioned in between CeHD stripes. **(C)** Relative positions of the epidermal supporting structures corresponding to the region in section #2. **(D)** Schematic illustration of CeHD components in the *C. elegans* epidermis. Among them, MUP-4 and MUA-3 are the apical transmembrane receptors; LET-805 is the receptor at the basement membrane; VAB-10A is the cytolinker that helps with the connection between the apical and basal CeHD units through the IFs.

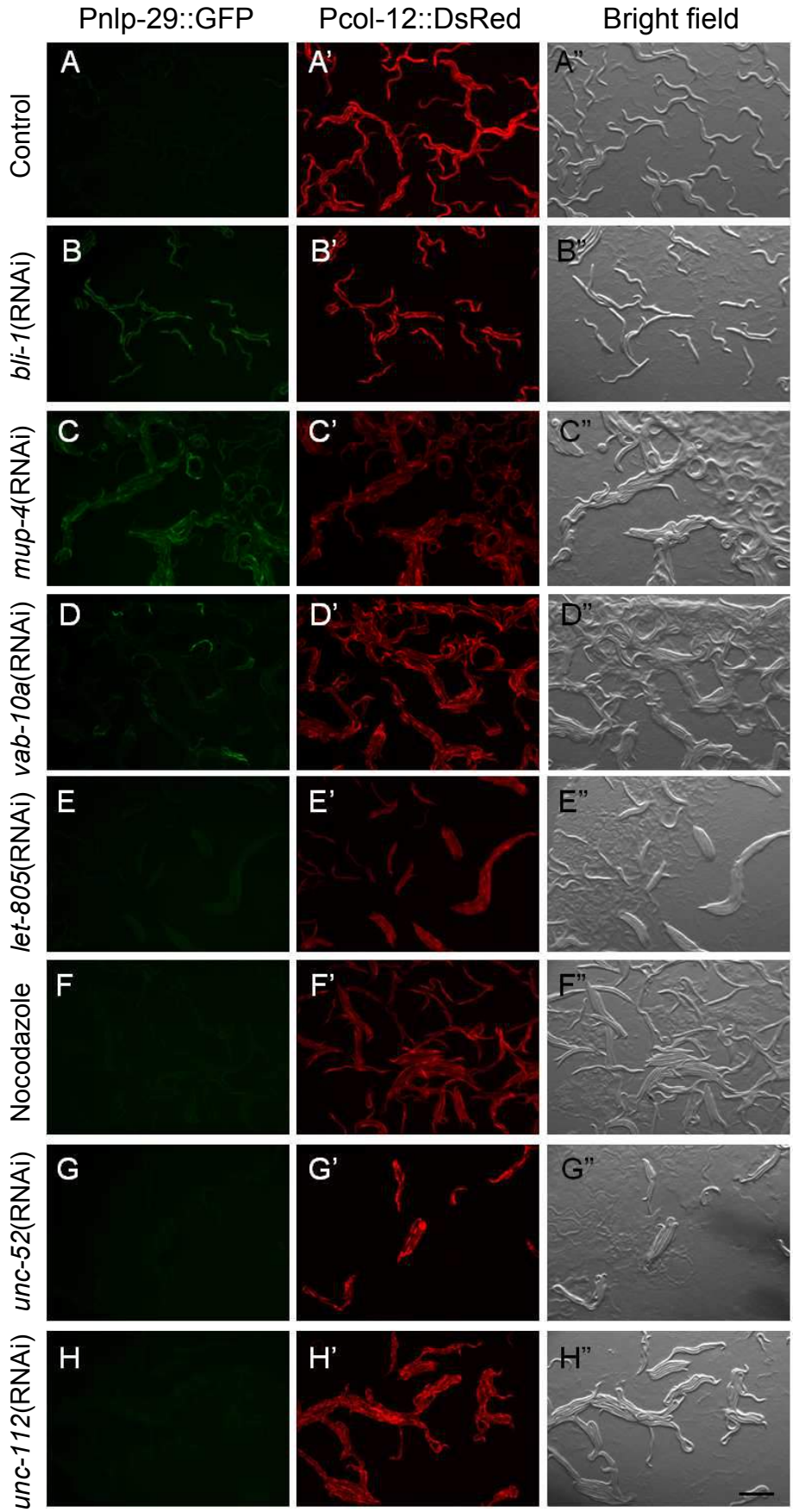

FigureS2: Change of *nlp-29* transcription level after disruption of different epidermal-supporting structures. Related to Figure 2

Worms carrying Pnlp-29::GFP in **(A)** wild-type control or after damage of **(B)** struts (*bli-1* RNAi), **(C)** apical CeHDs (*mup-4* RNAi), **(D)** plakin cytolinker (*vab-10a* RNAi), **(E)** basal CeHDs (*let-805* RNAi), **(F)** microtubule cytoskeleton (nocodazole), **(G)** basal ECM (*unc-52* RNAi) and **(H)** muscles (*unc-112* RNAi). Pcol-12::DsRed serves as internal control. Bright field images display locomotion and/or morphological defects caused by epidermal architectural damage. Note that for the control group, the positions of the worms in the three images (A-A", taken consecutively within seconds) are not identical because the worms were moving fast. In contrast, the RNAi or drug-treated worms display very little movement due to collapsed epidermis or muscles (B-H). Scale bar, 500μm.

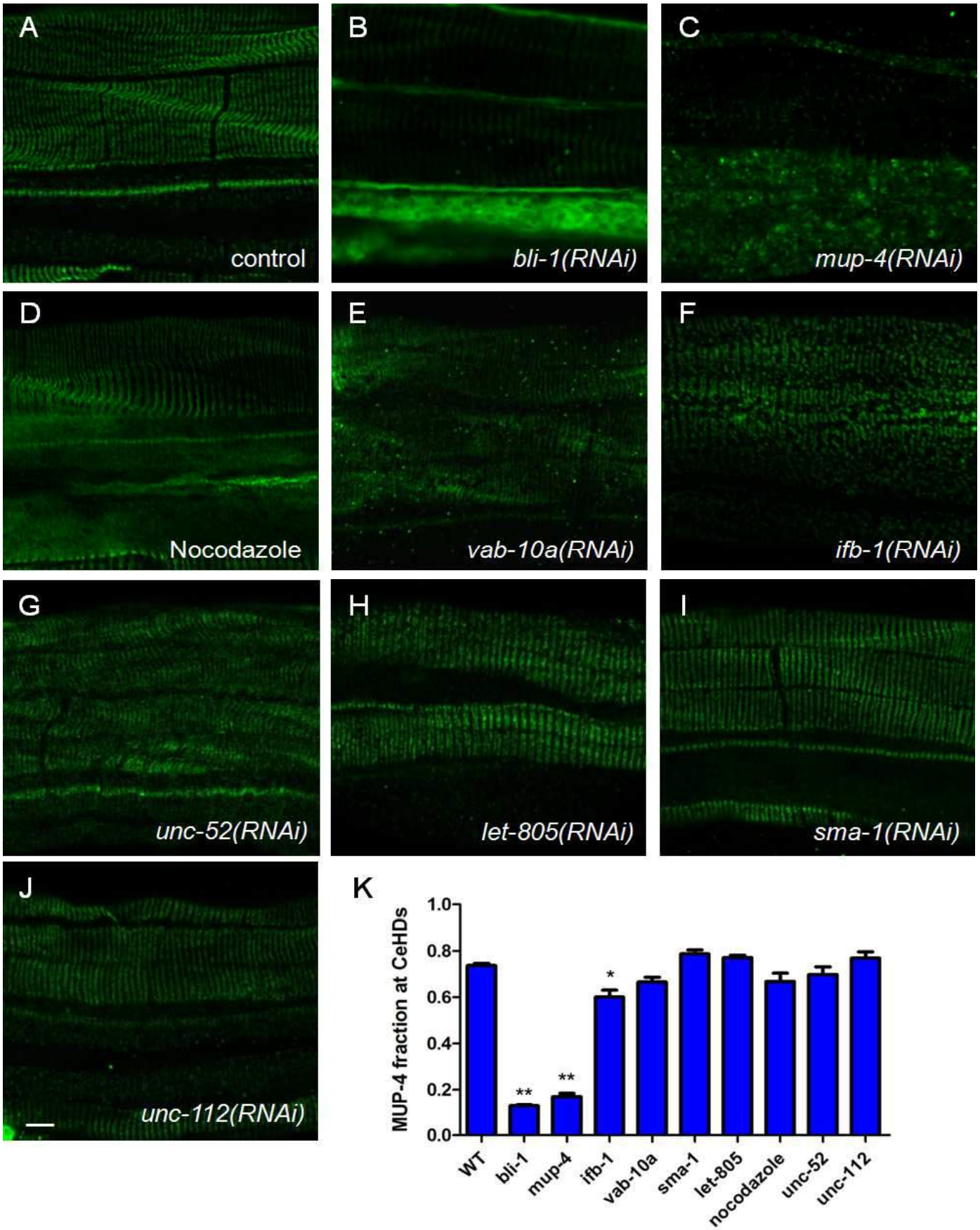

Figure S3. Defects of apical CeHD receptor MUP-4 localization following damage of different epidermal supporting structures. Related to Figure 3

(A-J) Representative confocal images of MUP-4 immunostaining in L4 hermaphrodites with damaged struts (*bli-1*), apical CeHDs (*mup-4*), cytolinker (*vab-10*), epidermal cytoskeletons (*ifb-1, sma-1* and Nocodazole), basal CeHDs (*let-805*), basal ECM (*unc-52*) or muscle structures (*unc-112*). The CeHD regions are the areas with parallel striped staining patterns located at the upper part of each image. Scale bar, 10μm. **(K)** Quantification of average MUP-4 signal intensity at the CeHD regions subtracted by the combined average intensity of MUP-4 at both CeHD and non-CeHD regions. The detailed quantification method is described in supplemental experimental procedures. Error bars, ±SEM. "*" denotes a significant decrease in the fraction of MUP-4 intensity at CeHDs compared with control. *, P<0.05; **, P<0.01.

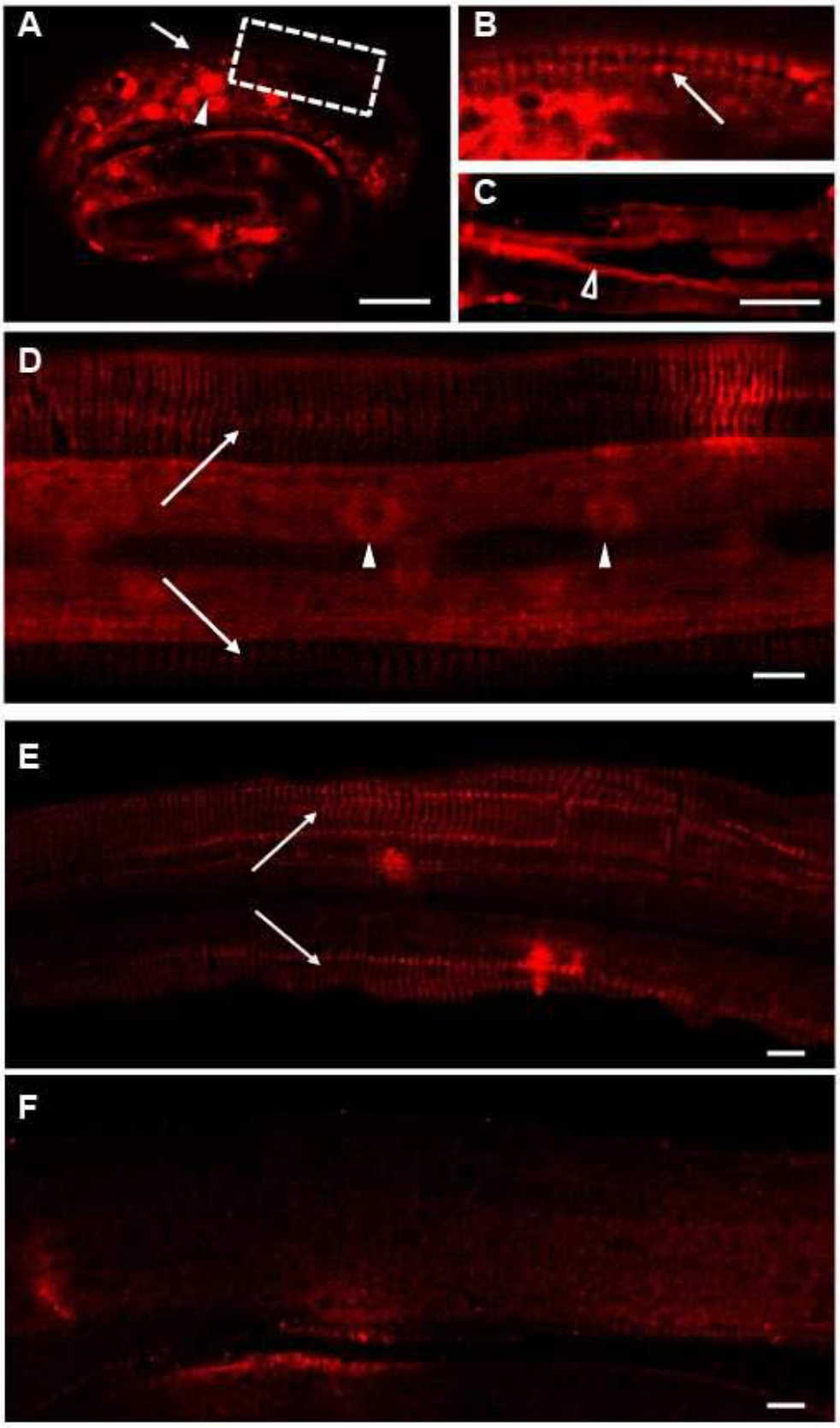

Figure S4: Localization of STA-2 in the epidermis at different development stages and different expression levels. Related to Figure 5

(A,B,D) Localization of mCherry::STA-2 driven by *sta-2* promoter in the epidermis. **(A)** The fusion protein is clearly visible in the CeHDs (arrow) and nuclei (arrowhead) from the embryonic stage. **(B)** Enlarged area corresponding to boxed region in (A). **(C)** STA-2 is enriched at the apical side (open arrowhead) of the pharyngeal epithelial cells, as shown by Pmyo-2::mCherry::STA-2. **(D)** Consistent with previous reports, mCherry::STA-2 driven by *sta-2* promoter is localized in the CeHDs (arrows) and nuclei (arrowheads) in L4 stage hermaphrodite. There is also diffused pattern seen in the cytoplasm. **(E-F)** STA-2 antibody staining of L4 stage hermaphrodite expressing endogenous STA-2 (E) and with *sta-2* expression inactivated by RNAi (F). Arrows in (E) point to STA-2 staining at CeHDs, which is mostly gone after *sta-2* knockdown (F). Scale bars, 10μm.

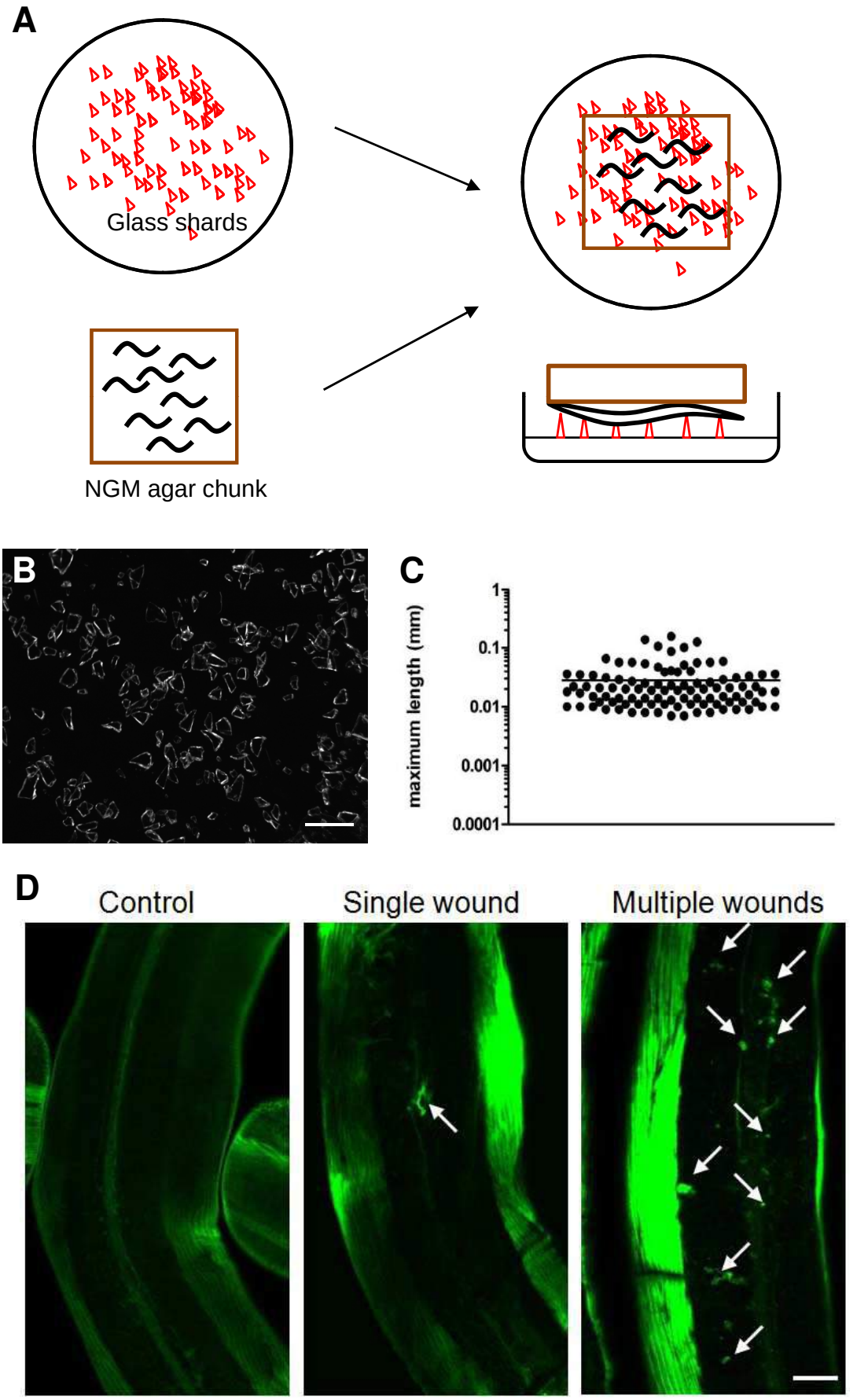

Figure S5: Severe physical injury approach in *C. elegans* epidermis. Related to Figure 6

(A) Diagram showing the principle of extensive wounding upon *C. elegans* epidermis. For detailed procedure see method section. **(B-C)** Appearance and size-distribution of the fine glass shards used for the wounding experiments. Maximum length refers to the length of the longest axis for each particle. Scale bar, 200μm. **(D)** Representative images of phalloidin-stained young adult worms with intact epidermis, a single wound produced by needle puncture or multiple wounds produced by glass shards. Arrows point to healing wounds in the epidermis marked by aggregated actin rings. Scale bar, 15 μm.

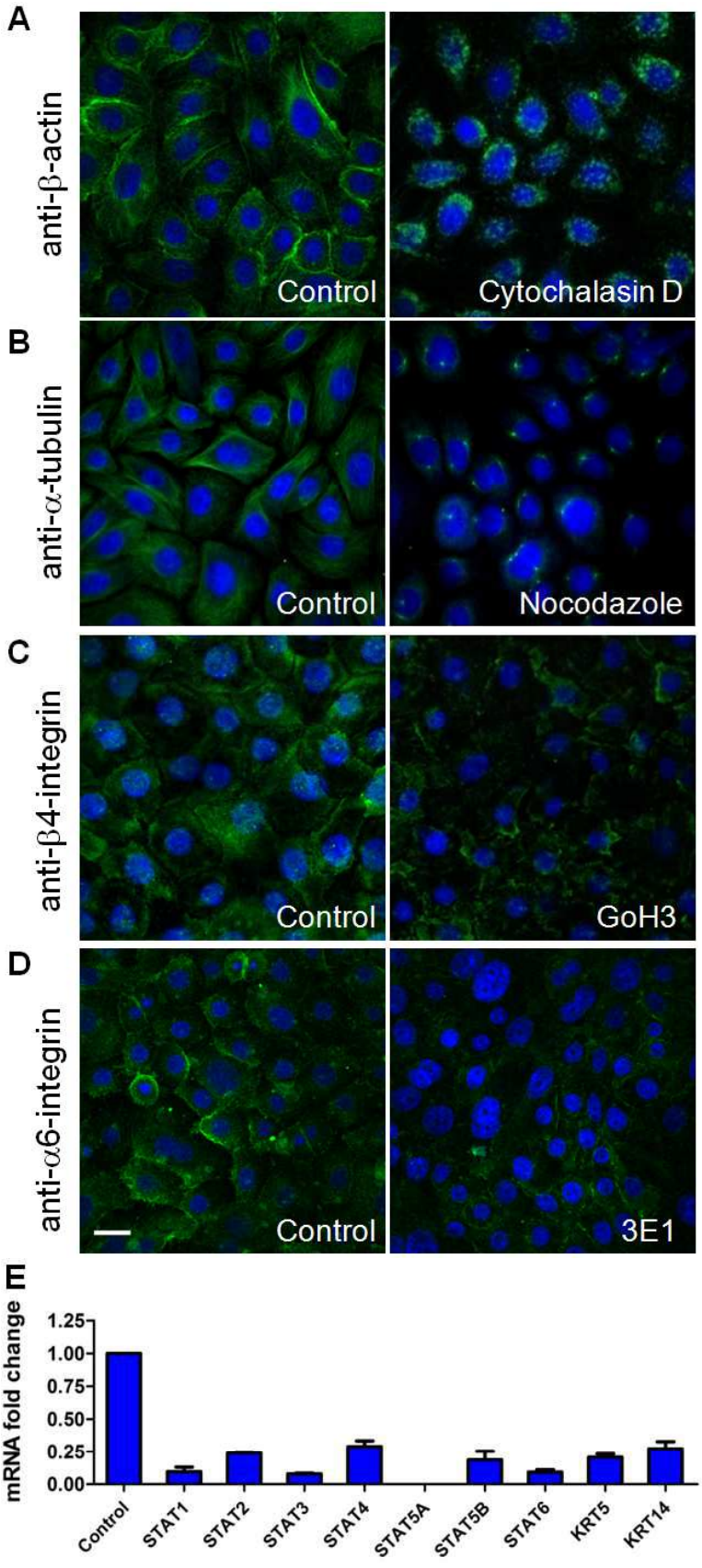

Figure S6: Disruption of supporting structures in primary human epidermal keratinocytes. Related to Figure 7

(A) Immunostaining of actin filaments with anti-β-actin antibody of primary HEKa cells with or without 200nM cytochalasin D (inhibitor of actin polymerization) treatment for 3 hours. **(B)** Immunostaining of microtubule bundles with anti-α-tubulin antibody of primary HEKa cells with or without 2μM nocodazole (inhibitor of microtubule polymerization) treatment for 3 hours. **(C)** Immunostaining of HPCs with anti-β4-integrin antibody in primary HEKa cells with or without 50μg GoH3 (blocking antibody of α6-integrin) treatment for 24 hours. **(D)** Immunostaining of HPCs with anti-α6-integrin antibody in primary HEKa cells with or without 50μg 3E1 (blocking antibody of β4-integrin) treatment for 24 hours. Scale bar, 25 μm. **(E)** siRNA knockdown efficiency test in HEKa cells by quantitative RT-PCR, showing the transcriptional reduction of each gene after siRNA knockdown compared to their own controls. The control expression levels of all the genes are normalized as one fold and displayed as a single bar on the left. Note that the transcript for STAT5A was no longer detected by RT-PCR after siRNA knockdown, therefore the value of which is presented as zero. Error bars, ±SEM.

SUPPLEMENTAL EXPERIMENTAL PROCEDURES

Strains and genetic methods

C. elegans strains were maintained at 20℃ as previously described (Brenner, 1974). The strains carrying *gpa-12(pk322), tir-1(tm3036), dbl-1(nk3), sma-6(wk7), sta-1(ok587), sta-2(ok1860), elt-3(gk121), sek-1(km4), pmk-1(km25), wnk-1(ok266), vab-19(e1036), pak-1(ok448), mua-3(rh195), eps-8(ok539), cgEx198[bli-1::GFP+unc-119(+)], upIs1[mup-4::GFP+pRF4(rol-6(su1006))]* and *frIs7[Pnlp-29::GFP+Pcol-12::DsRed]* were obtained from the CGC, which is funded by NIH Office of Research Infrastructure Programs (P40 OD010440). *git-1(tm1962)* was kindly provided by Hwai-Jong Cheng. To minimize intrinsic variation in Pnlp-29::GFP level, strain IG274 carrying *frIs7[Pnlp-29::GFP;Pcol-12::dsRed]* was outcrossed to N2 six more times and renamed HMZ009; strainsRB1547 carrying *sta-2(ok1860)* mutation and KU4 with *sek-1(km4)* mutation were crossed into HMZ009 background four times before analysis .

C. elegans RNAi and drug treatment

RNA interference was induced mainly by bacterial feeding using clones from the MRC RNAi library, after verifying the sequence of the corresponding inserts. *vab-10a* RNAi clone was constructed by inserting 544bp fragment within exon17 into the HindIII site of vector L4440 .For *bli-1, ifb-1 ,sma-1, unc-52* and *unc-112* RNAi, worms were fed with RNAi against those genes from the L1 stage. For *mup-4, vab-10a* and *let-805* RNAi, worms were fed with RNAi against those genes from the L2/L3 stage to prevent premature lethality. More than 90% penetrant morphological defects were observed at

late L4 stage, with minimum lethality occurred. For disruption of microtubule bundles, L4-stage wild-type worms were soaked in 60ug/ml nocodazole dissolved in M9 for 2hours, and then recovered in M9 buffer for 2 hours before collection. Control groups were soaked in M9 buffer for 4 hours before analysis.

Molecular biology and transgenesis

Translational Pdpy-7::mcherry::sta-2 fusion was generated by PCR-cloning 650bp *dpy-7* promoter fragment inserted upstream of mCherry, followed by 4073bp *sta-2* genomic sequence from ATG inserted downstream of mCherry into pPD49.78 vector. To drive mCherry::STA-2 in the pharynx, *dpy-7* promoter of Pdpy-7::mcherry::sta-2 fusion construct was replaced by 1230bp *myo-2* promoter fragment. To construct Psta-2::mcherry::sta-2 fusion, *dpy-7* promoter of Pdpy-7::mcherry::sta-2 fusion construct was replaced by 1995bp *sta-2* promoter fragment. Constructs used in this study were generated using ClonExpress TMOne Step Cloning Kit (Vazyme biotech). All fragments obtained by PCR amplification were confirmed by sequencing to double-check for mutations before transgenesis. Pmyo-2::mcherry::sta-2 was injected into N2 at a concentration of 15ng/µl. Pdpy-7::mcherry::sta-2 and Psta-2::mcherry::sta-2 *were* injected into *sta-2(ok1860)* at the concentration of 15ng/ul and 10ng/µl, respectively. Pmyo-2::GFP was used as co-injection marker.

Immunostaining and fluorescence microscopy of *C. elegans*

Worms were fixed and stained by indirect immunofluorescence as previously described (Costa et al., 1997). Dilution factors for primary antibodies are:

anti-GFP(DSHB-GFP-12A6), 1:25; anti-MUP-4, 1:500; anti-DPY-7, 1:500; anti-mCherry, 1:500; anti-intermediate filament(MH4), 1:50; anti-UNC-52(MH3), 1:300; anti-PAT-3(MH25), 1:100; anti-tubulin(AA4.3), 1:100; anti-LET-805/myotactin(MH46), 1:100; anti-STA-2, 1:50. 12A6, AA4.3 and MH mAbs were purchased from the DSHB (University of Iowa). The MUP-4 polyclonal antibody was raised against peptide PRAKLARPLYGDEMGDD as previously described (Hong et al., 2001).The STA-2 polyclonal antibody was raised against peptides CRNLAPDEIYFDNQGAAT and CVAEEFQHKKSASAEGDW, flanking the SH2 domain of STA-2 protein. Phalloidin staining of the epidermal actin filaments was performed as previously described (Costa et al., 1997). Single-plane fluorescent images were captured using Nikon A1 confocal microscope or Leica TCS SP5 confocal microscope. The image in Figure 1A was assembled from two confocal scans of adjacent areas in a single worm. All images were processed using ImageJ (http://rsb.info.nih.gov/ij/). For quantification of MUP-4 mis-localization following disruption of different epidermal supporting structures, average intensities of MUP-4 fluorescent signal within and outside of CeHD regions (assigned as region A and region B, respectively) on the epidermis were quantified using ImageJ. The fraction of MUP-4 intensities at CeHDs were calculated as the value of A/(A+B). For each treatment, images from 5 individual animals were used and measured three times each at different regions. The epifluorescence images of single worms were taken by Nikon 901 upright fluorescence microscope. Images of multiple worms were taken by Olympus SZX16 stereo microscope and Nikon 901 upright fluorescence microscope.

Co-immunoprecipitation with worm lysates

The transgenic strains carrying Pdpy-7::mCherry::STA-2 and integrated MUP-4::GFP transgene or GFP alone were used to study the interaction of STA-2 and MUP-4. The co-IP experiment was performed following the protocol kindly provided by Mengqiu Dong's lab (NIBS, Beijing). Briefly, adult worms were collected and washed three times with M9 buffer. After snap-freezing in liquid nitrogen two times, the dry pellets were mixed with 2X pre-cooled lysis buffer (40mM Tris-HCl pH8.0,300mM NaCl,0.2% NP40,4mM EDTA) supplemented with protease inhibitor cocktails (ROCHE). After 5 minutes grinding on the ice with a hand-held homogenizer, the mixture was centrifuged at 12000rpm for 10mins at 4 ℃ to collect the supernatant. The lysates were centrifuged at 12000rpm for another 30 minutes at 4℃ then pre-cleared with Protein G PLUS-Agarose (SANTA CRUZ). The resulting lysates were then incubated with anti-GFP rabbit polyclonal antibody (SANTA CRUZ) at 4℃ for 10h, followed by incubation with Protein G PLUS-Agarose at 4℃ overnight. The complexes were then harvested by centrifugation and washed extensively with 1X lysis buffer before boiled for SDS-PAGE analysis. The antibodies used for immunoblotting were anti-GFP mouse mAb (MILLIPORE) and anti-mCherry Rat mAb(INVITROGEN). The secondary antibodies used were goat-anti-mouse IRDye 800 CW(C31021-01) and goat-anti-rat IRDye 680 RD (C30529-04) purchased from LI-COR. The odyssey SA imaging system was used for documentation of the western results.

qRT-PCR analysis

For quantitative RT-PCR analysis, total RNA was extracted by the RNAiso plus reagent (TakaRa) and reverse transcribed by primescript RT master mix (TakaRa). The realtime PCR reaction was performed using Faststart universal SYBR Green master(Roche) on Mastercycler EP realplex (Eppendorf). The primers for *C. elegans* samples are: act-1-F, TCCTTACCGAGCGTGGTTAC; act-1-R, GTTTCCGACGGTGATGACTT; nlp-29-F, TCCTTCTCGCCTGCTTCA; nlp-29-R, CTTTCCCCATCCTCCATACA;cnc-2-F, TGATGGGAGGTTATGGAGGA;cnc-2-R,GAGCATTCCAAGGAGTCCAG;sta-2-F,CTTG GTTTATGGGTTTTGCAG;sta-2-R,ATCGACGTCGGAGAACTTGT. The primers for HEKa samples are: gapdh-F, GAGTCAACGGATTTGGTCGT; gaphd-R, GACAAGCTTCCCGTTCTCAG. hCAP18-F, CCAGGTCCTCAGCTACAAGG; hCAP18-R, TCTGGTGACTGCTGTGTCG. hBD2-F, CCAGCCATCAGCCATGAGGGT; hBD2-R, GGAGCCCTTTCTGAATCCGCA. hBD3-F, CTTCTGTTTGCTTTGCTCTTCC; hBD3-R, CACTTGCCGATCTGTTCCTC.IL6-F, AGACTTGCCTGGTGAAAATCA;IL6-R, AAAGCTGCGCAGAATGAGAT. IL8-F, GTGCAGTTTTGCCAAGGAGT;IL8-R, ACTTCTCCACAACCCTCTGC. TNF-F, GAGCACTGAAAGCATGATCC;TNF-R, GCCAGAGGGCTGATTAGAGA. KRT5-F, CAATCTGCAGAACGCCATT;KRT5-R, TGCCATATCCAGAGGAAACA. KRT14-F, TCACAGCCACAGTGGACAAT; KRT14-R, CCTCTCAGGGCATTCATCTC.STAT1-F, TGATGTTTCATTTGCCACCA; STAT1-R, TGAATATTCCCCGACTGAGC. STAT2-F, TAATCTCCAGGAACGGAGGA; STAT2-R, GGCTCTATCACAGGCTCCAG. STAT3-F, TTTGTCAGCGATGGAGTACG; STAT3-R, GCTGCAACTCCTCCAGTTTC. STAT4-F, AACCATGGCAACGATTCTTC; STAT4-R, GCTGCAGCCAATATTCTCCT. STAT5a-F, GCCATTGACTTGGACAATCC;STAT5a-R,

GGCAGCGGTCATATGTTTTC. STAT5b-F, TCTGATGCCTTTTACCACC;STAT5b-R, TGCTTGATCTGTGGCTTCAC. STAT6-F, ACCCACCACACTCTCACTCC;STAT6-R, GGTCACATCTGAGCAGAGCA.

Amplification program for all genes was as followed: 10 min at 95 °C, followed by 40 cycles for 15s at 95 °C, 30 s at 60 °C and 15s at 72 °C. Each experiment was repeated at least three times with cDNA templates derived from different RNA samples and each reaction was run in quadruplicate. Normalized against the reference gene *act-1*or *gapdh*, the expression levels of target genes relative to controls were calculated using REST 2009 software (QIAGEN).Statistical analysis was performed using Prism 5.0 software (Graphpad Software, Inc). Significance was accepted for $P<0.05$ (student *t-test*).

Physical injury of the epidermis

Single-wound injury experiment for fluorescent imaging was carried out using microinjection needles mounted on Eppendorf Transferman NK2 micromanipulator. Large-scale needle wounding for QPCR analysis was operated by hand using microinjection needles mounted on a pen-holder and with worms on the NGM plates immobilized by pre-cooling on ice. Severe physical injury assay was performed by placing worms on a layer of fine glass shards. Specifically, glass shards with diameters ranging from 10-100um were produced by grinding 0.25mm-thick glass capillaries (Sutter, BF-100-50-10). Glass shards were then washed with and stored in 75% ethanol in a 15ml conical tube until use. Over- or under-sized shards were removed by gravity separation and filtration through 300 mesh sieve. The length of the longest axis

for each glass particle was measured and analyzed by ImageJ. NGM plates for injury were prepared by spreading glass shards evenly onto the plate, covering the entire agar surface. A chunk of NGM agar with hundreds of worms was then placed upside-down onto the glass shards, gently pressed, and let stay for 5min before moving the worms to new plates for recovery. This method does not cause significant lethality among treated worms. Injured worms were then transferred to fresh plates with OP50 and collected 1 hour later for phalloidin staining or 5 hours later for GFP imaging. Control worms were treated in the same way without the addition of glass shards.

Primary Human epidermal keratinocytes culture and treatments

The normal human epidermal keratinocytes-adult (HEKa, FC-0025) cell line is purchased from Lifeline cell technology. The HEKa cell was grown in DermaLife Basal Medium supplemented with DermaLife K LifeFactors, 100U/ml penicillin and 100U/ml streptomycin. Cells were grown at 37℃ in a humidified chamber with 5% CO_2.

Function blocking Mouse mAb P1B5 against α3-integrin(MAB1952P) and 3E1 against β4-integrin (MAB1964) were purchased from Millipore. Function blocking rat mAb GoH3 against the extracellular portion of α6-integrin (SC-19622) was purchased from Santa cruz. Mouse mAb A2-F6 against beta-actin(M1210-2) was purchased from HuaAn Biotechnology. Mouse mAb 1E4C11 against α-tubulin(66031-1-Ig) was purchased from Proteintech Group. siRNA reagents for gene knockdown were designed and synthesized by GenePharma Corporation. CytochalasinD and Nocodazole were purchased from Sangon Biotech. Inhibitors for p38-MAPK

(SB203580) and NF-kB (BAY11-7082) were purchased from Selleck Chemicals.

For drug treatment, 80% confluent HEKa cells were treated with 200nM cytochalasin D, 2μM nocodazole or DMSO control for 3 hours before gene expression analysis or immunostaining. For p38 and NF-κB inactivation, cells were treated with 1μM SB203580 or 10μM BAY11-7082 for 24 hours before analysis. For functional blocking of integrins, cells were treated with 50μg/ml blocking antibodies for 24 hours before analysis. For siRNA knockdown, transfections were performed with 100nm siRNA using Lipofectamine3000 (L3000-015) from Life Technologies. Transfection mixtures were replaced by DermaLife medium after 24 hours and incubated for an additional 24 hours before assayed for gene expression.

For immunostraining, HEKa cells grown and treated on Lab-Tek ^{TM}II Chamber Slide (Thermo) were fixed with ice-cold acetone for 10 minutes and permeabilized with 0.2% Triton X-100 in PBS for 10 minutes at room temperature. After three times rinsing with PBS, cells were blocked with 5% FBS for 30 minutes, then incubated with primary antibodies overnight at 4℃. Dilution factors for primary antibodies are 1:1500 for 3E1 and 1:100 for all other antibodies. Cells were subsequently incubated with secondary antibodies directed against mouse or rat IgG for 90 minutes at room temperature. The nuclei were counterstained with 0.1 ug/ml DAPI. The immunolabeled slides were mounted in DABCO and examined under Nikon A1 confocal microscope.